Additive Manufacturing 25 (2019) 365–389

Contents lists available at ScienceDirect

Additive Manufacturing

journal homepage: www.elsevier.com/locate/addma

Areal topography measurement of metal additive surfaces using focus variation microscopy

Lewis Newton[a,*], Nicola Senin[a,b], Carlos Gomez[a], Reinhard Danzl[d], Franz Helmli[d], Liam Blunt[c], Richard Leach[a]

[a] Manufacturing Metrology Team, University of Nottingham, NG8 1BB, UK
[b] Department of Engineering, University of Perugia, 06125, Italy
[c] University of Huddersfield, Huddersfield, HD1 3DH, UK
[d] Alicona Imaging GmbH, Graz, Austria

ARTICLE INFO

Keywords:
Additive manufacturing
Laser powder bed fusion
Electron beam powder bed fusion
Surface metrology
Focus variation microscopy

ABSTRACT

In this work, the performance of a focus variation instrument for measurement of areal topography of metal additive surfaces was investigated. Samples were produced using both laser and electron beam powder bed fusion processes with some of the most common additive materials: Al-Si-10Mg, Inconel 718 and Ti-6Al-4V. Surfaces parallel and orthogonal to the build direction were investigated. Measurement performance was qualified by visually inspecting the topographic models obtained from measurement and quantified by computing the number of non-measured data points, by estimating local repeatability error in topography height determination and by computing the value of the areal field texture parameter *Sa*. Variations captured through such indicators were investigated as focus variation-specific measurement control parameters were varied. Changes in magnification, illumination type, vertical resolution and lateral resolution were investigated. The experimental campaign was created through full factorial design of experiments, and regression models were used to link the selected measurement process control parameters to the measured performance indicators. The results indicate that focus variation microscopy measurement of metal additive surfaces is robust to changes of the measurement control parameters when the *Sa* texture parameter is considered, with variations confined to sub-micrometre scales and within 5% of the average parameter value for the same surface and objective. The number of non-measured points and the local repeatability error were more affected by the choice of measurement control parameters. However, such changes could be predicted by the regression models, and proved consistent once material, type of additive process and orientation of the measured surface are set.

1. Introduction

The layer-by-layer approach offered by additive manufacturing (AM) allows for the creation of complex geometries, reducing the need for assembly and increasing design freedom [1]. Common AM techniques for the production of metal additive manufactured parts include electron beam powder bed fusion (EBPBF) and laser powder bed fusion (LPBF) [2], and there are an increasing number of materials that are available as feedstock for PBF [3].

Surface topography measurement for metal additive manufacturing (AM) plays important roles, both for assessing the surface texture [4–10] and as a tool to investigate how the manufacturing process behaves by measuring the surface features produced (the manufacturing process signature, that is the 'fingerprint' left on the surface that makes the surface recognisable [11], albeit a complete signature has not been found yet for metal AM processes [12]. The challenge of finding reliable signatures is exacerbated by there being significant measurement challenges related to additive surfaces. For surfaces produced via PBF, measurement challenges are related to non-uniformity of optical properties, with highly reflective smooth regions appearing together with poorly contrasted, dark recesses, high aspect-ratio features, high slope angles and most critically undercuts [13,14], all of which vary dependent on relative build orientation, powder size and AM process used.

When investigating as-built surfaces, the top surface topography consists of the laser or electron beam melt paths and any spatter that may occur [15]. As-built side surfaces are a result of multiple layers adhering to one another whilst interacting with the powder bed around the part geometry, which may cause semi sintering of particles to these side

* Corresponding author.
E-mail address: lewis.newton@nottingham.ac.uk (L. Newton).

https://doi.org/10.1016/j.addma.2018.11.013
Received 27 August 2018; Received in revised form 19 October 2018; Accepted 9 November 2018
Available online 15 November 2018

surfaces [16]. For EBPBF, the as-built side surfaces are especially dominated by powder adhesion due to the need for the process to semi sinter a powder region around the part geometry into a 'cake'; this acts to offer support and increase thermal conductivity during the build process [17].

Previous work has indicated focus variation (FV) measurement technologies as providing a good compromise between quality of measurement results, versatility, ease of operation and measurement times [13,18–20]. These characteristics have resulted in FV being utilised in the measurement of metal additive surfaces [5,13,15,21–27]; however, further research is needed to identify optimal set-up configurations, and the actual influence of the available measurement process parameters on the final measurement results. This work form the basis of the presently reported study.

Contributing a further understanding of FV measurement of metal additive surfaces, to identify guidelines for the optimal operation of FV instruments, this work explores the sensitivity of FV measurement to selected, controllable measurement process parameters. The experimentation and results illustrated in the following were obtained on a variety of materials and metal AM processes. Measurements were performed using an Alicona InfiniteFocus (IF) G5 instrument, but the findings should be broadly applicable to any conventional FV instrument [20].

1.1. Background

FV utilises an optics with a limited depth of field combined with a vertical scanning process [18,20] (see Fig. 1). A sequence of images is recorded as the optics is moved vertically along the optical axis, resulting in a vertical image stack. For each pixel within an image, corresponding to a location in the *x*, *y* plane, a measure of local contrast is obtained by algorithmically combining information about the surrounding bright and dark pixels. The computation is repeated for the same pixel in all the images of the vertical stack. When the computations are complete, a series of contrast values (known as a contrast curve) is available for each *x*, *y* location, spanning the entire set of vertically stacked images. Additional algorithms are then used to determine the maximum contrast value for each curve, and its *z* location (which may be interpolated from the *z* values of the available images in the stack). The combined x, y, z information corresponding to the maximum contrast point in each curve is used to create a 3D point in the topography map, whilst the RGB colour information associated to the maximum contrast point at each location is used to generated a fully-focused colour map of the same surface.

FV is a relatively popular method to measure the surface topography of AM parts due to its ability to capture high slope angles while being reasonably robust to varying optical properties (e.g. reflectivity) [19]. In recent work, a 3D linear theory for FV is discussed, which investigates the various illumination settings available to the instrument (coaxial, ring light or polarised coaxial illumination) and their effects on measurement results [28]. Other work investigates illumination in FV while at the same time varying the tilt of the surface being measured and the lateral resolution of the measurement [29]. FV has been previously used to measure titanium alloy samples made using LPBF and EBPBF [5]; however, the settings of the instrument are mentioned but not systematically investigated. FV measurement has been investigated in comparison to other measurement technologies; in [9], where the same LPBF top surface is measured with FV, confocal chromatic microscopy, coherence scanning interferometry (CSI) and X-ray computed tomography, and the results are compared. Further investigation of how individual metal AM topographic features appear as measured via different technologies can be found elsewhere [15]. Investigative work into the effect of the instrument settings on the measurement of AM surfaces has been carried out for other optical surface measurement technologies, such as CSI [14].

2. Materials and methods

2.1. Samples

In this work, four samples produced by LPBF and EBPBF were inspected (Table 1 and Fig. 2). The blocks were built so that the top surface would be orthogonal to the build direction (referred to as 0° build orientation).

The surface roughness of the four samples were preliminary

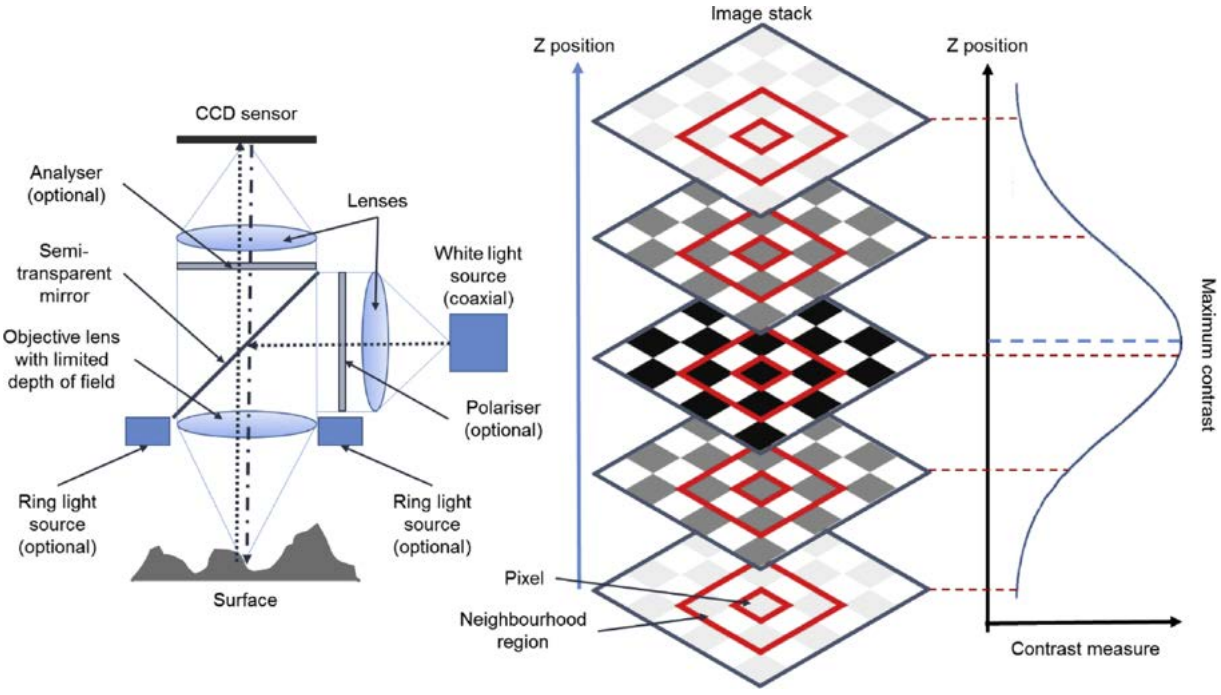

Fig. 1. Schematic diagram of the focus variation technology; a) elements of the optics system; b) images captured during vertical scanning, arranged as a stack. The small red square represents an example pixel where contrast is computed; the large red square represents the window of neighbouring pixels used to compute contrast c) the contrast curve associated to the example pixel, obtained by interpolation between contrast values from the image stack. The maximum of the curve (height measurement result) may not correspond to any reference height of the images in the stack. (For interpretation of the references to colour in this figure legend, the reader is referred to the web version of this article).

Table 1
Sample block material, commercial machine, and sample part size.

Material	Commercial system	Build properties
Al-Si-10Mg aluminium alloy	Renishaw AM250	(20 × 20 × 20) mm cube
Inconel 718 nickel super-alloy	Renishaw AM250	(50 × 20 × 15) mm block
Ti-6Al-4 V titanium alloy	Renishaw AM250	(20 × 20 × 20) mm cube
Ti-6Al-4 V titanium alloy	Arcam 2XX	(70 × 20 × 15) mm block

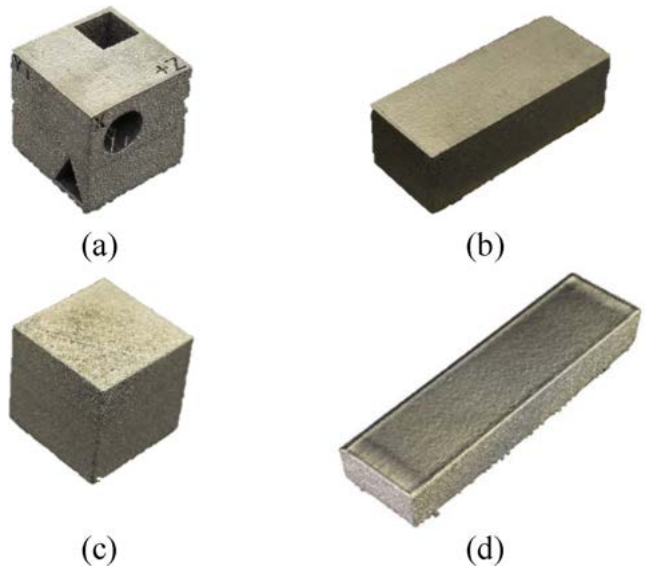

Fig. 2. Samples: (a) Al-Si-10Mg LPBF cube, (b) Inconel 718 LPBF block, (c) Ti-6Al-4 V LPBF cube, and (d) Ti-6Al-4 V EBPBF block.

assessed via the ISO 4287 [30]roughness parameter *Ra*, the arithmetical mean deviation of the assessed profile using a contact stylus instrument (TalySurf FormIntra50, 2 µm tip diameter, 0.5 µm sampling distance) as shown in Table 2. In Table 2, each *Ra* is reported as an arithmetic mean ± standard deviation over a series of 10 parallel profiles measured orthogonally to the main texture direction, with 3.3 mm evaluation length, levelling by least-squares mean line subtraction, low-pass filtering for noise removal (cut-off wavelength λ_s 2.5 µm) and high-pass filtering for waviness removal (cut-off wavelength λ_c 2.5 mm).

Despite profile roughness parameters not being directly comparable to the quantitative assessment results obtainable from optical instruments and pertaining areal topography, the Ra results reported in Table 2 offer a first, reference insight on the texture of the sample surfaces.

2.2. Process parameters for the optical measurement

The samples were measured using an Alicona Infinite Focus G5, simply referred to as "FV instrument" henceforth. The following measurement process instrument parameters were considered:

Table 2
Values of the ISO 4287 roughness parameter *Ra* for the surfaces of the test samples (arithmetic mean ± std. deviation).

Surface	Roughness parameter, *Ra* / µm
Al-Si-10Mg LPBF top surface	15.8 ± 2.5
Al-Si-10Mg LPBF side surface	23.9 ± 4.7
Inconel 718 LPBF top surface	6.2 ± 1.3
Inconel 718 LPBF side surface	18.7 ± 1.8
Ti-6Al-4 V LPBF top surface	25.6 ± 3.2
Ti-6Al-4 V LPBF side surface	19.7 ± 2.9
Ti-6Al-4 V EBPBF top surface	6.7 ± 1.8
Ti-6Al-4 V EBPBF side surface	26.8 ± 3.2

Table 3
Selected FV measurement process parameters and their values. FoV is field of view and NA is numerical aperture.

Magnification	10× NA 0.3 FoV (1.62 × 1.62) mm	20× NA 0.4 FoV (0.81 × 0.81) mm	50× NA 0.6 FoV (0.32 × 0.32) mm
Illumination type	Coaxial Polarised coaxial Ring light	Coaxial Polarised coaxial Ring light	Coaxial Polarised coaxial Ring light
Lateral resolution/ µm	2, 4	1–3	1, 2
Vertical resolution/ nm	100, 300, 900	50, 200, 500	20, 50, 200

- magnification;
- illumination type;
- lateral resolution, and
- vertical resolution.

The magnifications considered were 10×, 20× and 50×, obtained by switching objective lenses (information in Table 3). The illumination types were: coaxial (light travelling along the same optical path as the FV probe), polarised (coaxial with a polariser [5] to reduce saturation effects due to strong specular reflection [6]) and ring light (ring-shaped light emitter to increase the input aperture of illumination and thus the amount of light captured at the detector even in the presence of high local slopes [28]). The choice of magnification directly affects the lateral and vertical resolutions that could be tested within each measurement set-up.

Vertical resolution is a term used by the FV instrument to specify distances between images in the focal image stack (Fig. 1). Because the vertical scanning is a continuous motion, vertical resolution as defined for the instrument relates to the sampling rate of images capture in the focal stack. Lateral resolution is a term used by the FV instrument to control the size of the region within which the contrast for each point is determined within each image of the stack.

Both terms vertical resolution and lateral resolution, as defined within the FV instrument, are prone to be misunderstood as they stray away from their more common interpretations. In areal topography measurement, vertical resolution is commonly accepted as the capability of resolving different height values, whilst lateral resolution is the capability of an instrument of resolving the different heights of two neighbouring points. This is clearly different from the definitions of vertical and lateral resolution adopted by the FV instrument and used in this work, as reported above. Whilst there is a relationship between vertical and lateral resolution as intended by the FV instrument and as commonly accepted, such relationship is not straightforward and not easy to elicit, given the multiple proprietary algorithms implemented by the FV instrument to obtain topography information from contrast. For example, vertical resolution intended by the instrument as the vertical spacing between images in the focal stack, is clearly related to the final capability of the instrument of resolving different height values. However, the resolution process passes through the construction of an interpolated contrast curve and the identification of its maximum, processes that are only partially disclosed by the instrument manufacturer. A similar process links the size of the window used to compute contrast and the lateral resolving power finally achieved by the instrument. In this paper, it was chosen to stick to the terminology adopted by the instrument manufacturer, to favour usability of the results.

2.3. Experimental plan

An experimental plan was designed to assess the influence of the selected measurement process parameters (magnification, illumination type, lateral resolution and vertical resolution) on the FV measurement results, with respect to application to metallic, AM surfaces. In Table 3, the

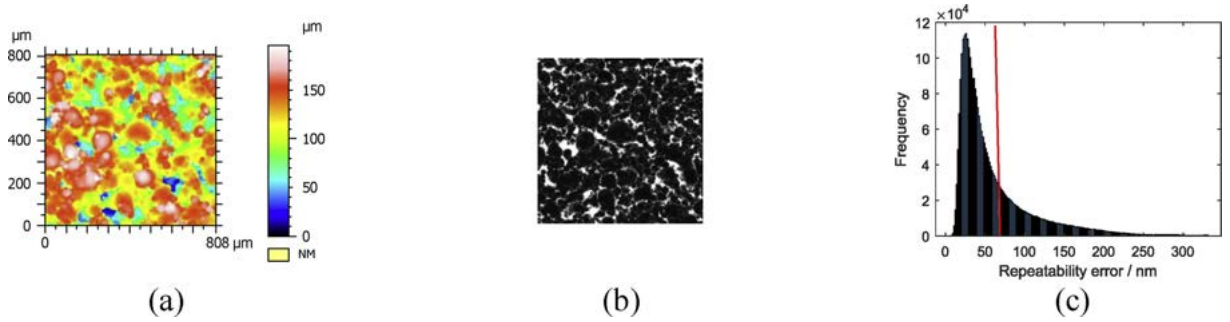

Fig. 3. Example computation of Q3, the upper quartile of the repeatability error (SLM Inconel 718 side surface measured using 20× objective, coaxial light, vertical resolution at 200 nm and lateral resolution at 2 µm); a) height map; b) quality map; c) probability distribution of the local repeatability error with the position of the upper quartile indicated by the red line (For interpretation of the references to colour in this figure legend, the reader is referred to the web version of this article).

measurement control parameters and their values are shown. Lateral and vertical resolution values were chosen considering the ranges automatically suggested by the instrument software once the proper magnification had been selected. The suggestions are based on proprietary algorithms of the instrument manufacturer, unfortunately not disclosed to the public. For lateral resolution, the default suggested value was taken as the largest value, and one or two (depending on magnification) smaller values (higher resolutions) were chosen, remaining within the range of acceptable values as suggested by the instrument software. For vertical resolution, the default suggestion by the instrument software was taken as the central value, together with one lower and one higher value, also within the range of acceptable values suggested by the instrument software.

From each one of the four samples described in Table 1 and shown in Fig. 2, both the top surface and one of the side surfaces were selected for measurement (one region per surface), leading to a total of eight regions being measured for each instrument set-up. For each region, three measurements were performed in sequence, in repeatability conditions (i.e. same set-up and position of the probe over the region), leading to a total of twenty-four measurements per set-up. A total of sixty-three set-ups were investigated, considering the combinations of measurement control parameters illustrated in Table 3, leading to a grand total of 1512 measured datasets.

2.4. Indicators of measurement performance

Each measurement by the FV instrument produced a height map (structured grid of height values, i.e. the topography dataset), an RGB colour map (2D image of colour as given by the optical probe, mapped to the same co-ordinates as the height map, and obtained in focus-stacking mode) and a quality map (structured grid reporting an estimate of the local repeatability error associated to each height point, as computed by the FV instrument itself; computation based on proprietary algorithms by the instrument manufacturer, undisclosed to the public). The following information was extracted/computed from the datasets as quality indicators.

a) 3D topography models reconstructed from the height maps and RGB colour maps.

The height maps were converted into triangle meshes and artificially coloured based on local height information. Additional models were created using the RGB colour map as texture overlays on top of the triangle meshes. Both types of models were 3D rendered for interactive visual inspection, to acquire an initial assessment of the quality of the datasets.

- NMP - percentage of non-measured points.

Within each height map, points for which the instrument does not acquire sufficient information were flagged by the instrument itself as non-measured. The second quality indicator, the percentage of non-measured points, was obtained as the ratio of non-measured points (as indicated by the instrument) over the total number of points of a topography dataset (in percentage).

- Q3 - Upper quartile of the distribution of the repeatability errors associated to each measured point.

The quality map produced by the FV instrument was used to build a probability distribution of local repeatability error in height determination. The upper quartile value (Q3) of such a distribution was used as an indicator of overall quality. Q3 represents the reference value for repeatability error below which 75% of the measured points are located (Fig. 3), so smaller Q3 values indicate better instrument performance (lower repeatability error).

- *Sa* – arithmetical mean height of the scale-limited surface.

The ISO 25178-2 areal field texture parameter *Sa*, the arithmetical mean height of the scale-limited surface [31,32], essentially a measure of local roughness, was considered. To compute the parameter, each dataset was processed with a form-removal operator (ISO 25178-2 F-operator) consisting of subtraction of the least-squares mean plane. No further filtering was performed (i.e. no separation of texture components at different spatial wavelengths). The procedure for computing *Sa* is not strictly ISO compliant, because of the limited size of the regions the parameter was computed on. The results are acceptable for comparison purposes, but may not necessarily agree with other literature on surface metrology for AM [10]. Topography data processing and texture parameter computations were carried on by using MountainsMap by Digital Surf [33].

2.5. Data analysis

For each magnification and for each one of the eight surface regions (Table 1, Fig. 2), three independent, general full factorial designs of experiments (DOEs) were generated for Q3, NMP and *Sa* respectively, to determine the sensitivity of the quality indicators to the factors: illumination type, vertical resolution and lateral resolution (levels previously illustrated in Table 3). From each DOE, regression models were fitted, and results were investigated by looking at the main effects plots and the statistical significance through ANOVA. For every regression model, the R-squared (R^2) statistics (the coefficient of determination, i.e. the proportion of the variance in the dependent variable that is predictable from the independent variables) was inspected to assess the goodness of the model. Also, for every independent variable (factor), the p-value was reported to indicate significance of that variable in affecting the result ($p < 0.05$ indicating that changes in the factor value do indeed trigger changes in the response variable).

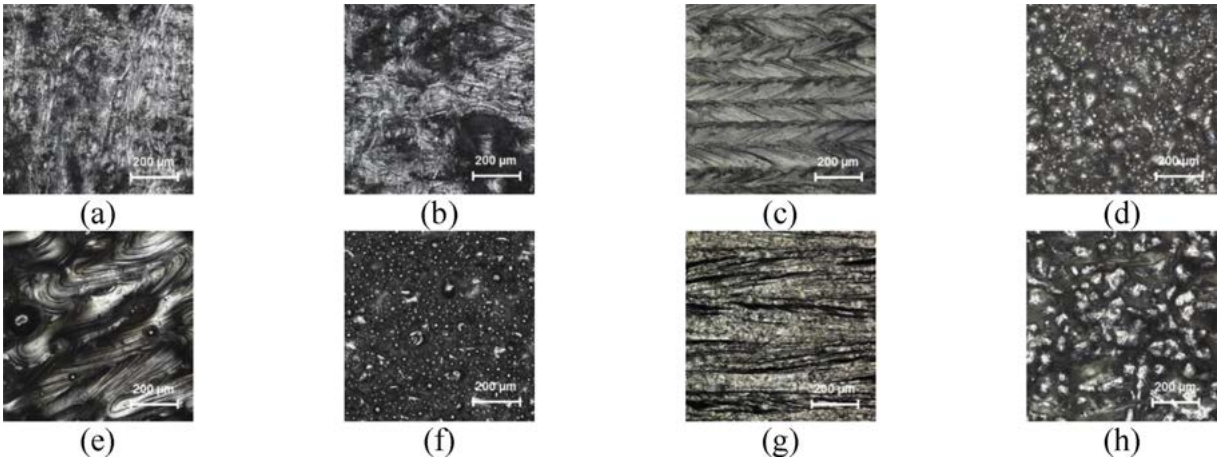

Fig. 4. Top views of topography models with RGB colour map overlays measured using 20× magnification, coaxial light, vertical resolution at 200 nm and lateral resolution at 2 µm; top surface (a) and side surface (b) for LPBF aluminium; top surface (c) and side surface (d) for LPBF nickel super-alloy; top surface (e) and side surface (f) for LPBF titanium alloy; top surface (g) and side surface (h) for EBPBF titanium alloy. Note that despite the surfaces having been rendered in colour (with the RGB map overlay), they visually appear as predominantly gray under the chosen illumination conditions.

3. Results

3.1. Visual investigation of the topography models

Top views for a selection of the specimens viewed by means of the RGB colour map overlays are shown in Fig. 4. These maps indicate some of the measurement challenges encountered when applying the FV technology to AM surfaces featuring dark, poorly contrasted recesses and specular oversaturated plateaus. As height detection in FV is based on contrast, such surfaces offer a number of challenges. The surfaces also appear very different depending on process (LPBF or EBPBF) and whether they are top or side surfaces. The side surfaces in particular present a much larger number of attached particles, which are typically very smooth and specular. Many features also possess high aspect ratios, or high local slopes, presenting an extra challenge to measurement. The evident diversity between surface types should be noted, with topographies varying significantly depending on process, material and build orientation. This last point is a further obstacle towards the identification of a single measurement set-up which may work optimally for all surfaces.

3.1.1. Effect of changing magnification

Topography models obtained using height-based colouring are shown in Fig. 5, for an EBPBF titanium top surface as an example. The use of different objectives leads to different surface features being captured depending on observational scale. The choice of magnification is clearly dependent on investigation goals. As can be seen in the height maps in Fig. 5, lower magnification objectives allow the capture of patterns formed by multiple weld tracks generated by the additive process (further details elsewhere [15]), as well as underlying larger-scale waviness components. At higher magnification objectives, smaller scale features, such as weld ripples, become more visible, despite there being limits to the best possible lateral resolution (smallest resolution value) due to both the optical resolution limit (related to the NA values reported in Table 3), and to the algorithms used by FV to resolve local height information by contrast detection [18].

3.1.2. Effect of changing vertical resolution

Height maps of the same surface obtained at different vertical resolution settings are shown in Fig. 6. Changes in vertical resolution have a significant effect on measurement time (higher resolution results in slower measurement). In terms of the effects of vertical resolution on height computation, according to the principle of operation of FV, higher resolutions (smaller resolution values) lead to the generation of a higher number of images in the vertical stack produced by vertical scanning. This should lead to a higher probability of detecting a point of maximum contrast in one of the stacked images. On the contrary, lower vertical resolutions produce fewer images in the stack, leading to a higher reliance on interpolation by the maximum contrast identification algorithm. In terms of visual inspection, as shown in Fig. 6, changes of vertical resolution produce few appreciable topographic differences.

3.1.3. Effect of changing lateral resolution on surface topography measurement

The lateral resolution setting is related to how many adjacent pixels are used to compute contrast and thus resolve local height. Changing lateral resolution (lateral scales measurable) produces a visible effect in the reconstructed height maps (see Fig. 7), despite the size of the covered area remaining the same when magnification is not changed. Higher lateral resolution leads to an increased level of lateral detail visible in the height map which can be used to reconstruct smaller features, such as the weld ripples and adhered particles. On the contrary, lower resolutions appear to introduce a smoothing effect on topography, due to larger overlapping windows used to determine local contrast.

3.1.4. Effect of changing illumination type on surface topography measurement

As visible in the RGB images of the surface shown in Fig. 8(a–c), each illumination type results in a different appearance of the same surface. Since such appearances are what is ultimately used by the FV technology to resolve height information through contrast detection, it is useful to see how different RGB appearances correlate with differences in the respective height maps. As shown in Fig. 8(d–f), the height maps produced under coaxial, polarised and ring light illumination contain visible differences. These can be explained by looking at the corresponding RGB images, where a different number of low-contrasted regions can be seen. Low-contrast regions may correspond to overly dark spots (insufficient illumination), overly bright spots (too much reflected light, causing saturation at the detector), or uniformly coloured spots (e.g. the abundance of gray areas in Fig. 8b). The net result is that higher spatial frequency topography components appear more pronounced under coaxial and polarised coaxial light illuminations than with the ring light. In Fig. 8e the polarised coaxial illumination setting also appears to contain extreme peaks in the measurement, which are likely due to the capture of a highly reflective features which affect the determination of local contrast, shown as bright regions in Fig. 8b, influencing the overall range of the detected height values.

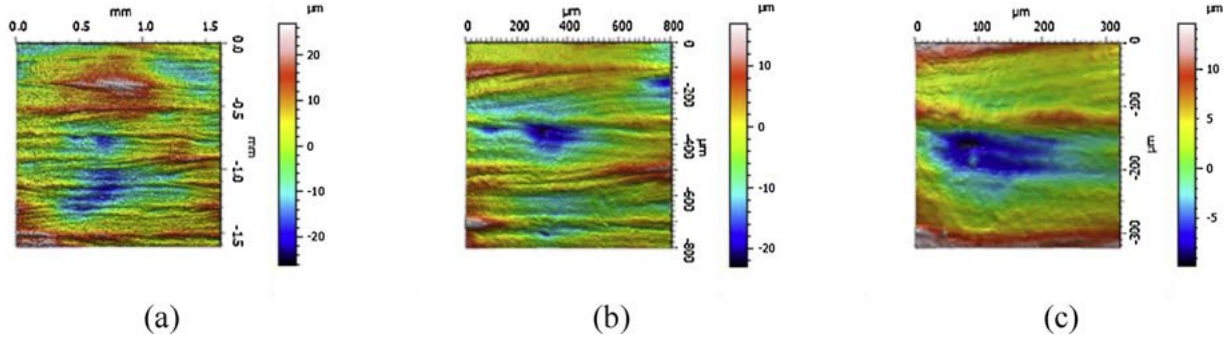

Fig. 5. Height map visualisation of an EBPBF titanium alloy top surface measured using coaxial light at (a) 10× magnification, (b) 20× magnification, and (c) 50× magnification.

3.2. General full factorial DOE

In this section, only the relevant results pertaining Q3, NMP and *Sa* are illustrated. The complete results are reported as supplementary material in Appendix A.

3.2.1. Results for Q3

3.2.1.1. Quality of model fitting. For the 10× magnification, R^2 was above 90% in all cases except for the Inconel 718 LPBF top (71.5%) and Ti-6Al-4 V LPBF top (87.3%). For the 20× magnification, R^2 was above 90% in all cases except Inconel 718 LPBF top (76.3%). For the 50× magnification, R^2 was above 90% in all cases except Inconel 718 LPBF side (82.9%) and Ti-6Al-4 V LPBF top (60.8%). In summary, a good fitting was obtained for the majority of cases, but not for all of them.

3.2.1.2. Main effect plots. At 10× magnification (Fig. 9), vertical resolution was the only significant factor ($p < 0.05$). In all cases, Q3 increased with larger vertical resolution values (lower resolution).

At 20× (Fig. 10), vertical resolution was still a significant factor (as for the 10× magnification) and Q3 still increased with vertical resolution values in all cases. However, lateral resolution was also found to be a significant factor, albeit Q3 varied much less with lateral resolution and there was no consistent trend (in several cases it decreased, in a few cases oscillated, in a small number of cases increased).

At 50× magnification (Fig. 11), vertical resolution was found as the only significant factor (as for the 10× magnification). Q3 increased at lower vertical resolution, in all cases.

3.2.1.3. Summary. For Q3, the full factorial models fitted well. The worse fitting performance was for Inconel 718 LPBF top, followed by Ti-6Al-4V LPBF top, and by Inconel 718 LPBF side. At all magnifications, vertical resolution was the most significant factor, and Q3 always increased at lower vertical resolution. This is presumably due to the presence of a larger number of images in the focal stack, useful for a more accurate detection of the maximum contrast point for each pixel. Illumination type was never a significant factor. Lateral resolution was significant only at 20×, albeit with limited influence on Q3 when compared to vertical resolution.

3.2.2. Results for NMP

3.2.2.1. Quality of model fitting. At 10× magnification, R^2 >was above 80% only for Inconel 718 LPBF top, with the worst fitting for the Al-Si-10Mg LPBF side (73.1%). At 20× magnification, R^2 was above 80% only for Inconel 718 LPBF side (84.1%), with the worst fitting for Al-Si-10Mg LPBF top (55.6%). Similarly, at 50× magnification, R^2 was above 80% only for Ti-6Al-4V LPBF top (81.3%), Ti-6Al-4V LPBF side (90.6%) and Ti-6Al-4V EBPBF side (82.5%) with the worst fitting for Ti-6Al-4V EBPBF top (72.7%). In summary, the full factorial models for NMP were characterised by relatively good fitting.

3.2.2.2. Main effect plots. At 10× magnification (Fig. 12), illumination type and lateral resolution were found to be significant. For illumination type, except for Al-Si-10Mg which showed no consistent trend, for top surfaces, higher NMP were observed with coaxial and lower NMP with ring illumination, whilst the opposite was observed for side surfaces. Concerning lateral resolution, NMP always decreased, with lower lateral resolution.

At 20× magnification (Fig. 13), lateral resolution was still

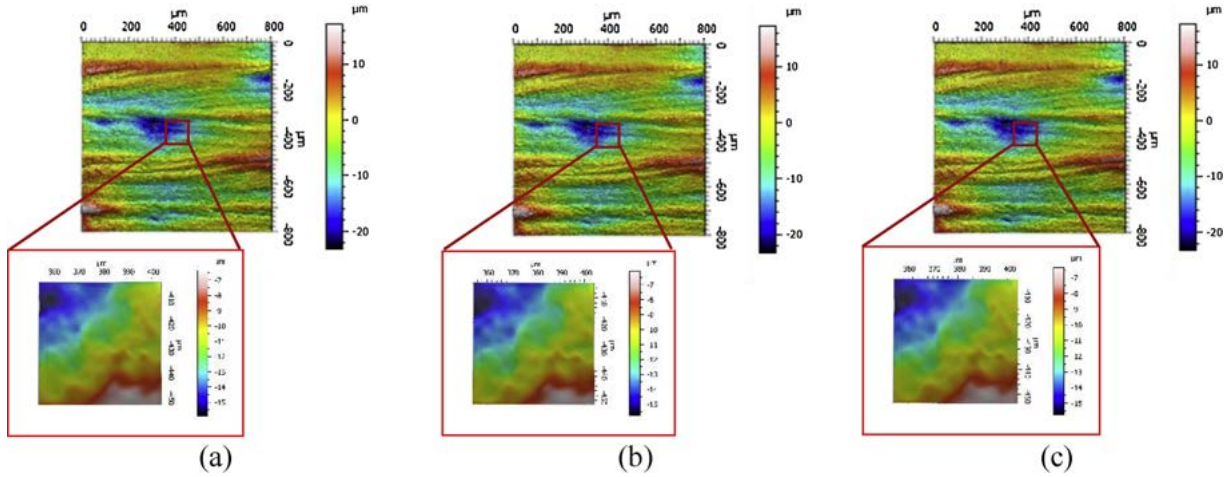

Fig. 6. Height map visualisations of an EBPBF titanium alloy top surface measured using 20× magnification, coaxial light, lateral resolution at 2 µm, and vertical resolution at (a) 50 nm, (b) 200 nm and (c) 500 nm.

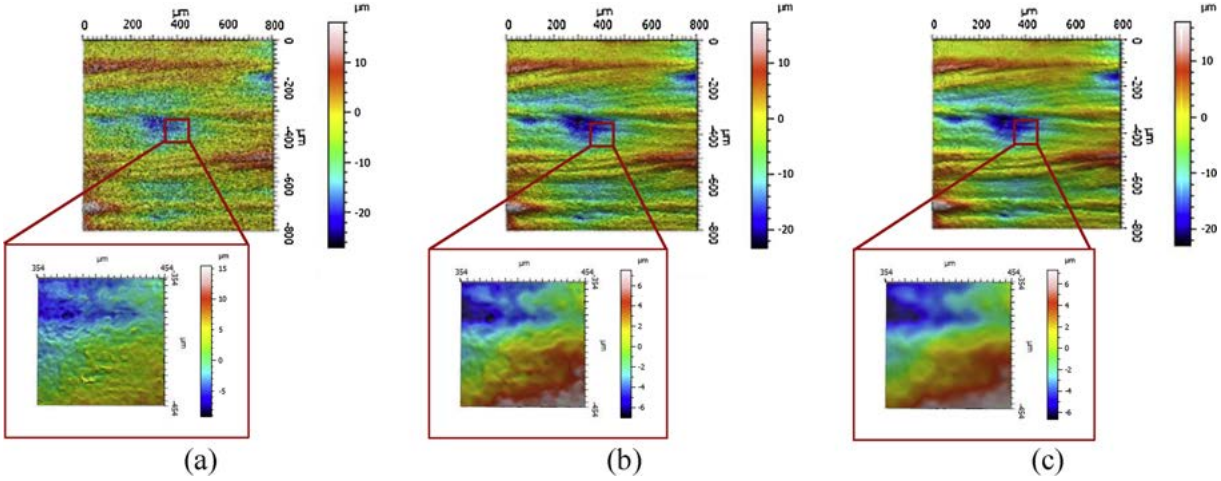

Fig. 7. Height map visualisation of EBPBF titanium alloy top surface measured using 20× magnification, coaxial light, vertical resolution at 200 nm, and lateral resolution at (a) 1 µm, (b) 2 µm and (c) 3 µm.

significant (as at 10× magnification), with lower lateral resolution still leading to decreasing NMP. Illumination type was not found significant, but vertical resolution was, almost as important as lateral, with lower vertical resolutions also leading to a decrease of NMP.

At 50× magnification (Fig. 14), the same situation was observed as at 20× magnification. Lateral resolution was found significant, and NMP decreased with lower lateral resolutions as previous. Vertical resolution was also found to be significant, and usually as the resolution became lower, NMP decreased, as with 20× magnification.

3.2.2.3. Summary. For NMP, lateral resolution was observed as a consistently relevant factor at all magnifications: reducing lateral resolution lead to decreasing NMP. Illumination type was only significant at 10×, but with inconsistent effects (i.e. varying with surface orientation and type of material). Vertical resolution was significant at 20× and 50× magnifications, with lower resolution leading to decrease in NMP as observed for lateral resolution.

3.2.3. Results for the surface texture parameter Sa

3.2.3.1. Quality of model fitting. At 10× magnification, R^2 was above 98% in all cases, with six out of eight models above 99%. At 20× magnification, R^2 was above 83% in all cases except for Al-Si-10Mg LPBF top (76.1% and for five cases R^2 was above 90%. At 50× magnification, R^2 was above 90% in all cases except for Al-Si-10Mg LPBF side (80.5%) and Ti-6Al-4 V LPBF side (82.9%). In summary, the full factorial models for *Sa* were characterised by relatively good fitting.

3.2.3.2. Main effect plots. At 10× magnification (Fig. 15), lateral resolution was significant, with lower lateral resolution leading to a decrease of *Sa*, except for in two cases, where it led to a slight increase (although never more than 0.5 µm). Illumination type was the other significant factor, with *Sa* decreasing from coaxial to polarised to ring illumination, except for two cases. Variations of *Sa* obtained when changing settings within the limits of the DOE were confined within a micrometre in most cases.

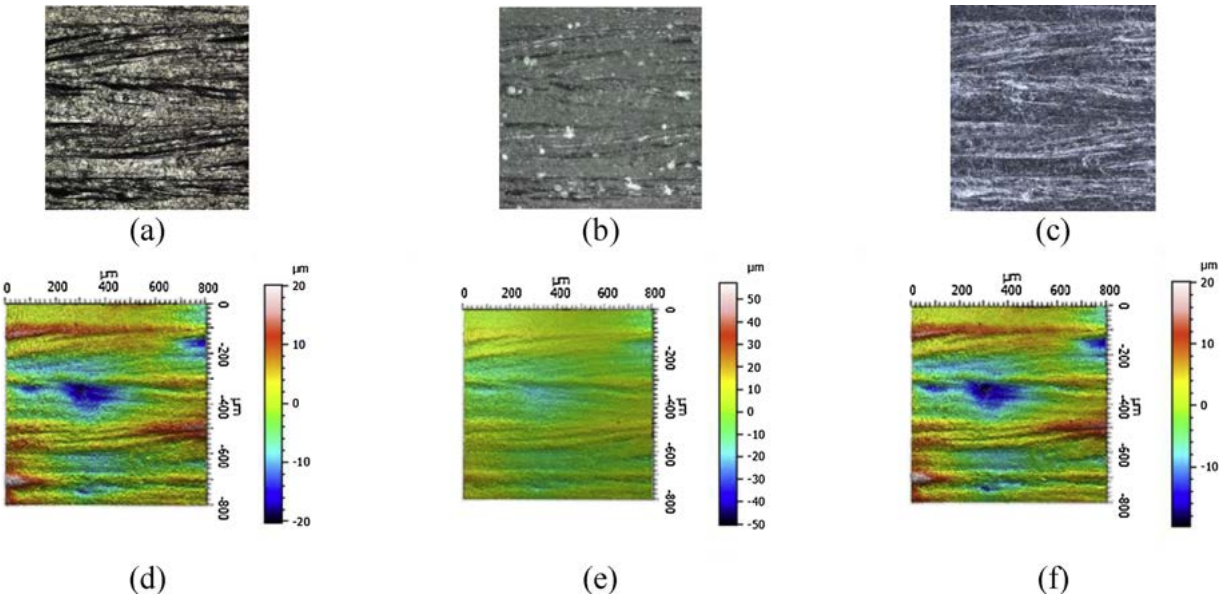

Fig. 8. EBPBF titanium alloy top surface measured using 20× magnification, lateral resolution at 2 µm, vertical resolution at 200 nm; focus stacked RGB images using (a) coaxial light, (b) polarised coaxial light and (c) ring light illumination. Corresponding height maps using (d) coaxial light, (e) polarised coaxial light and (f) ring light illumination.

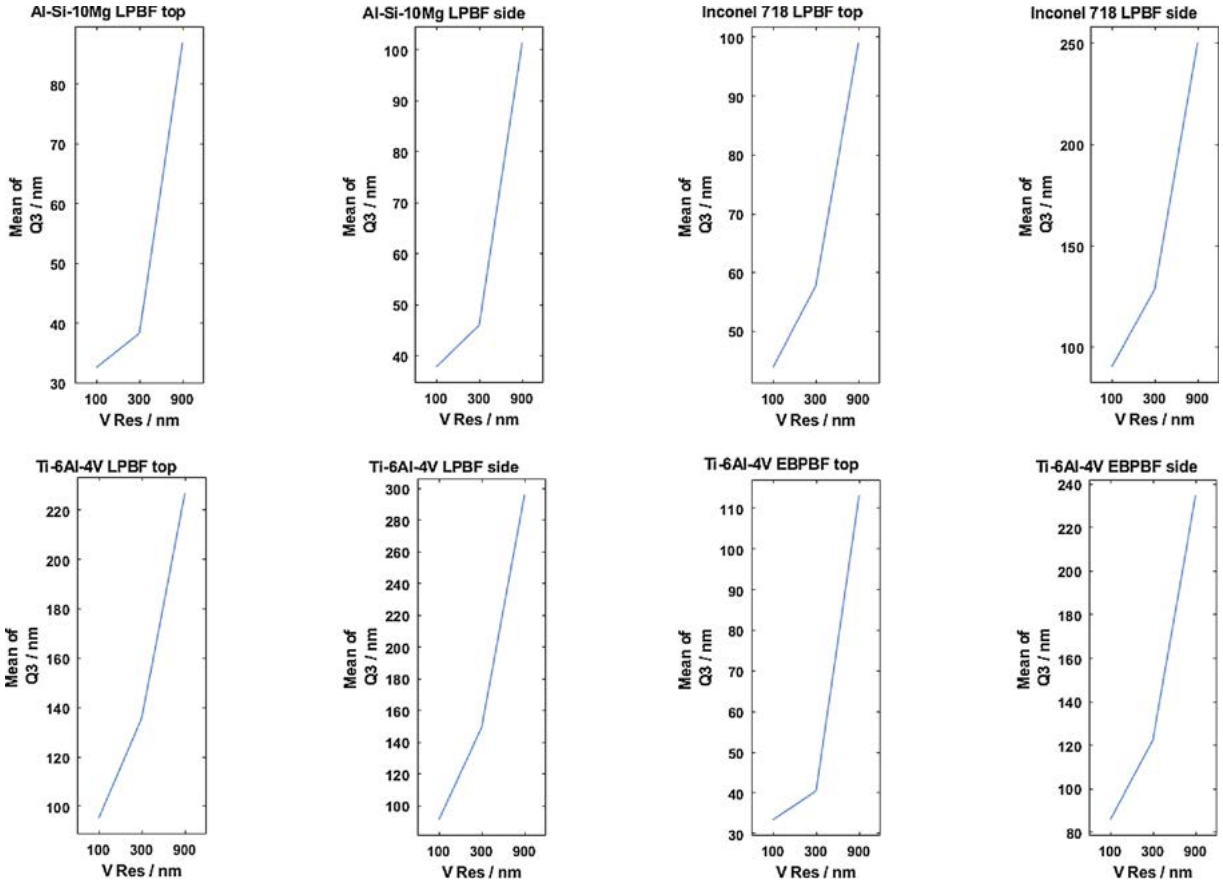

Fig. 9. Main effect plots for Q3 at 10× magnification.

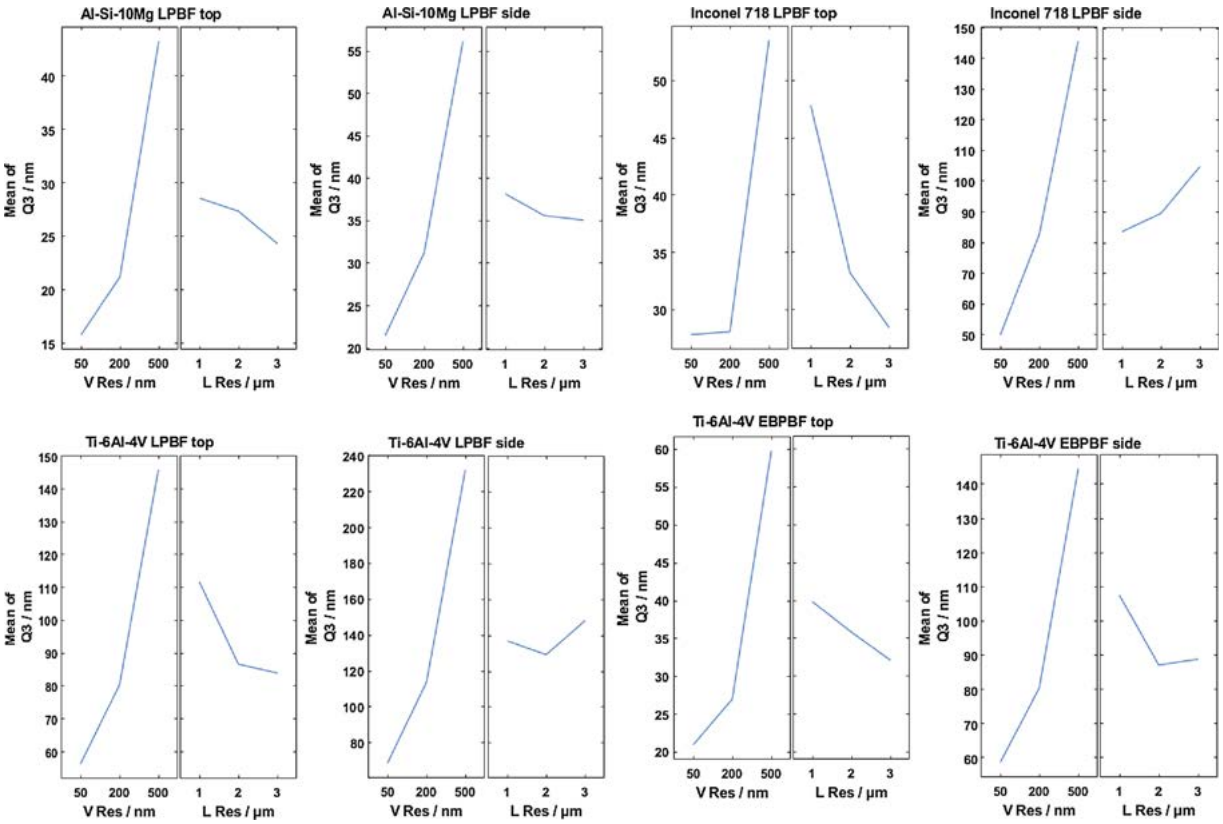

Fig. 10. Main effect plots for Q3 at 20× magnification.

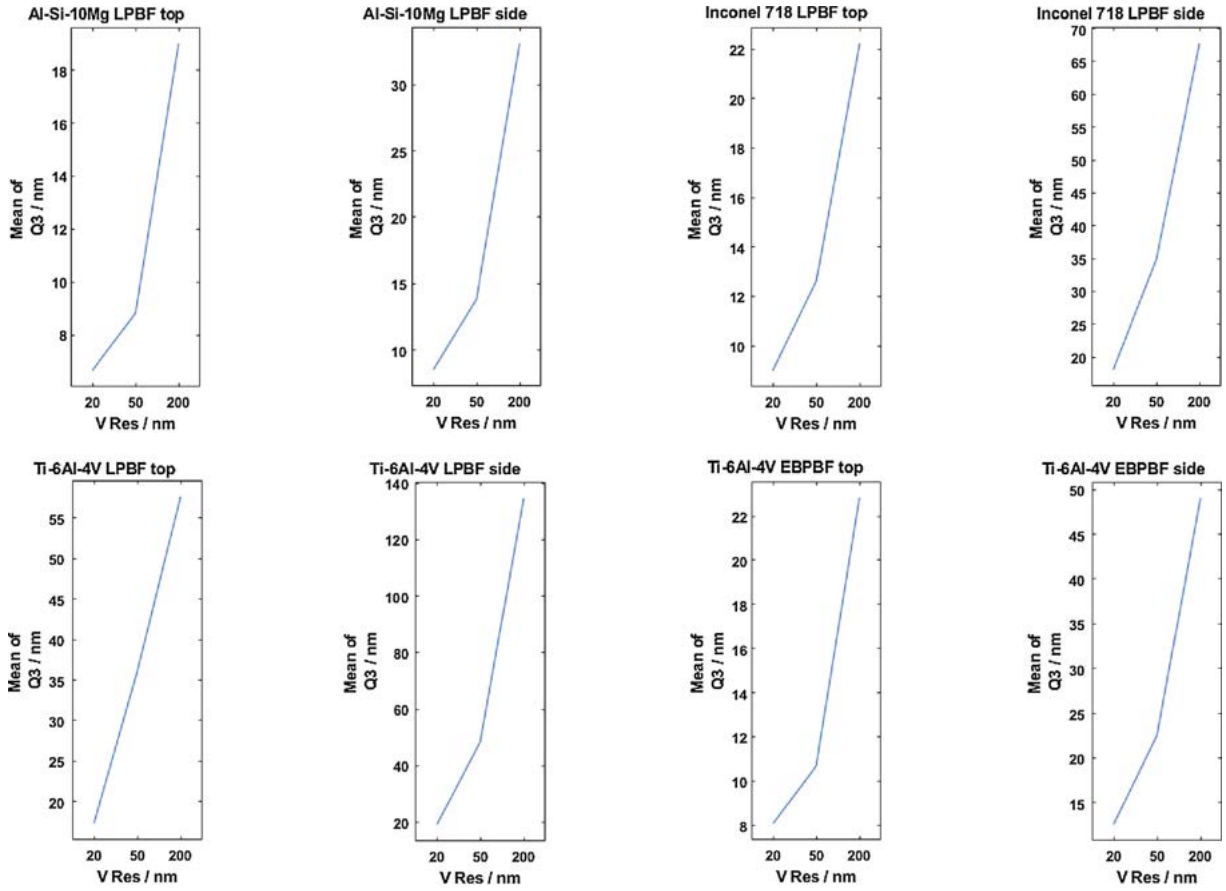

Fig. 11. Main effect plots for Q3 at 50× magnification.

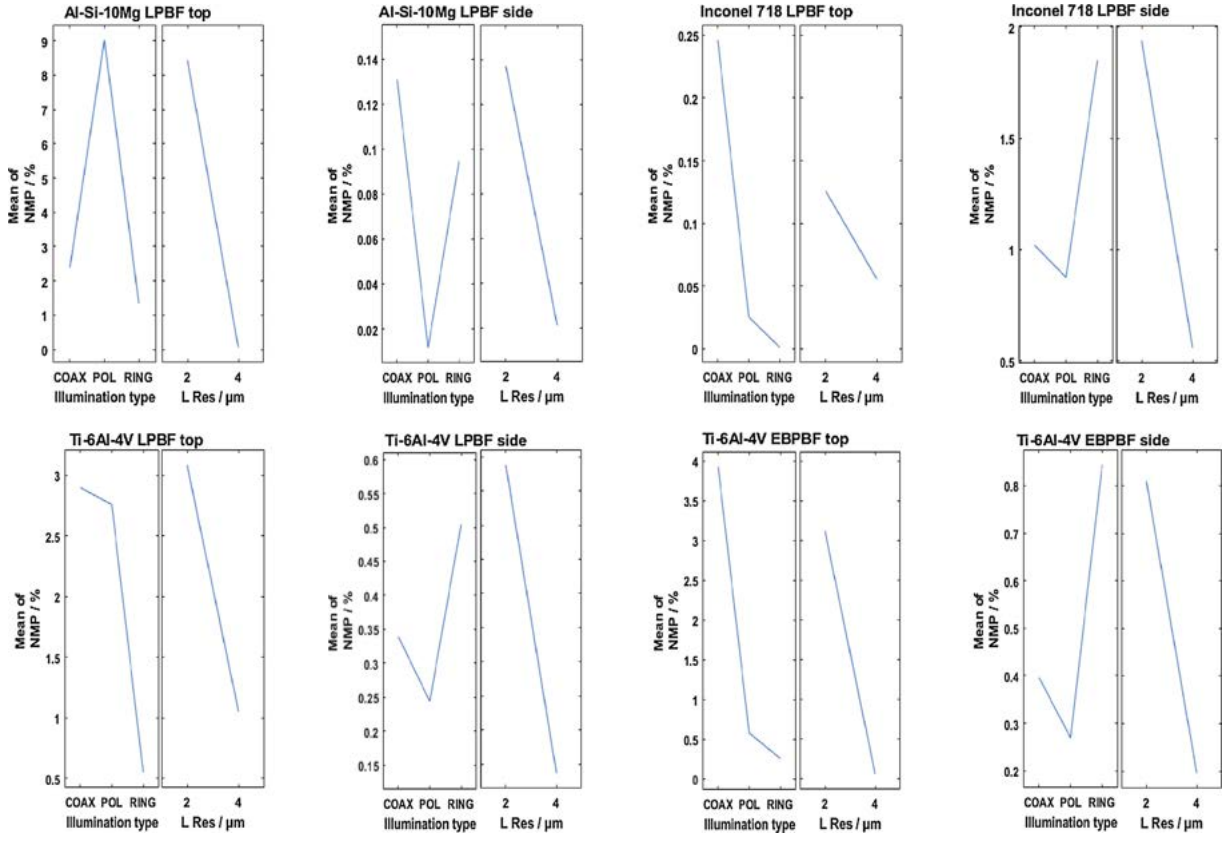

Fig. 12. Main effect plots for NMP at 10× magnification.

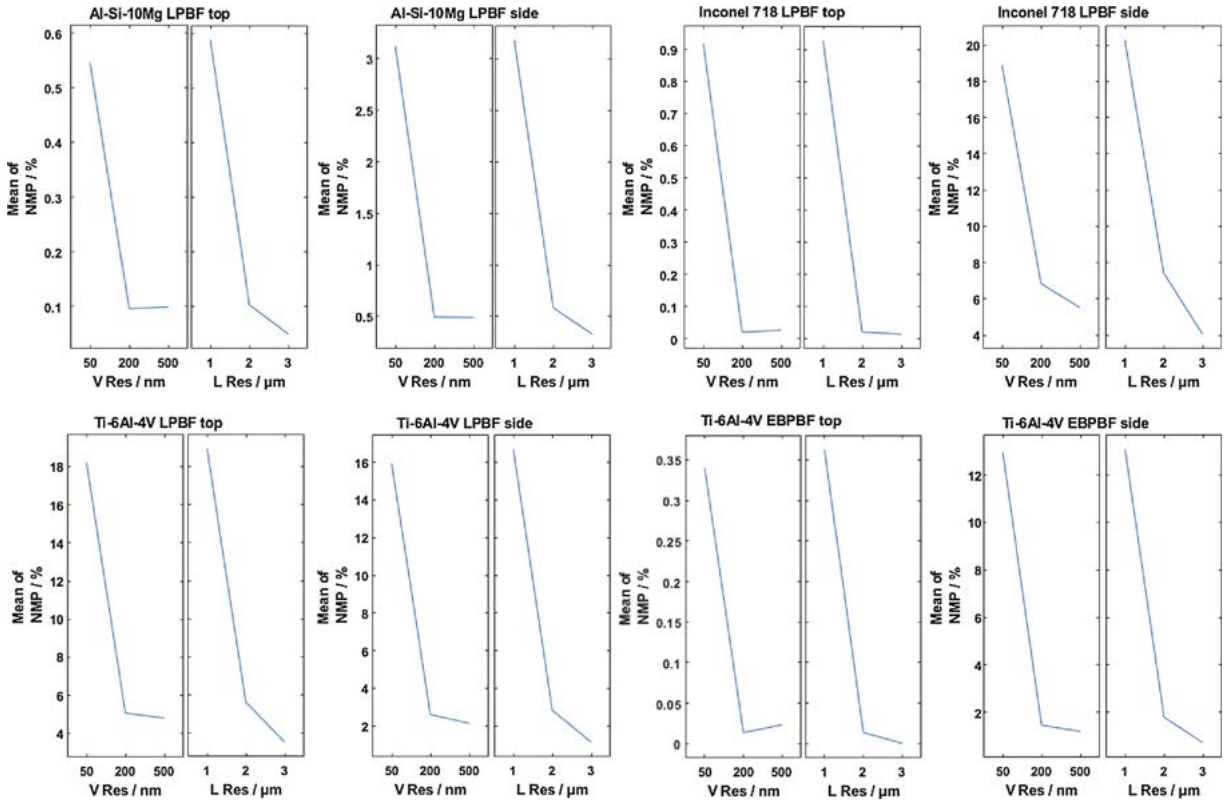

Fig. 13. Main effect plots for NMP at 20× magnification.

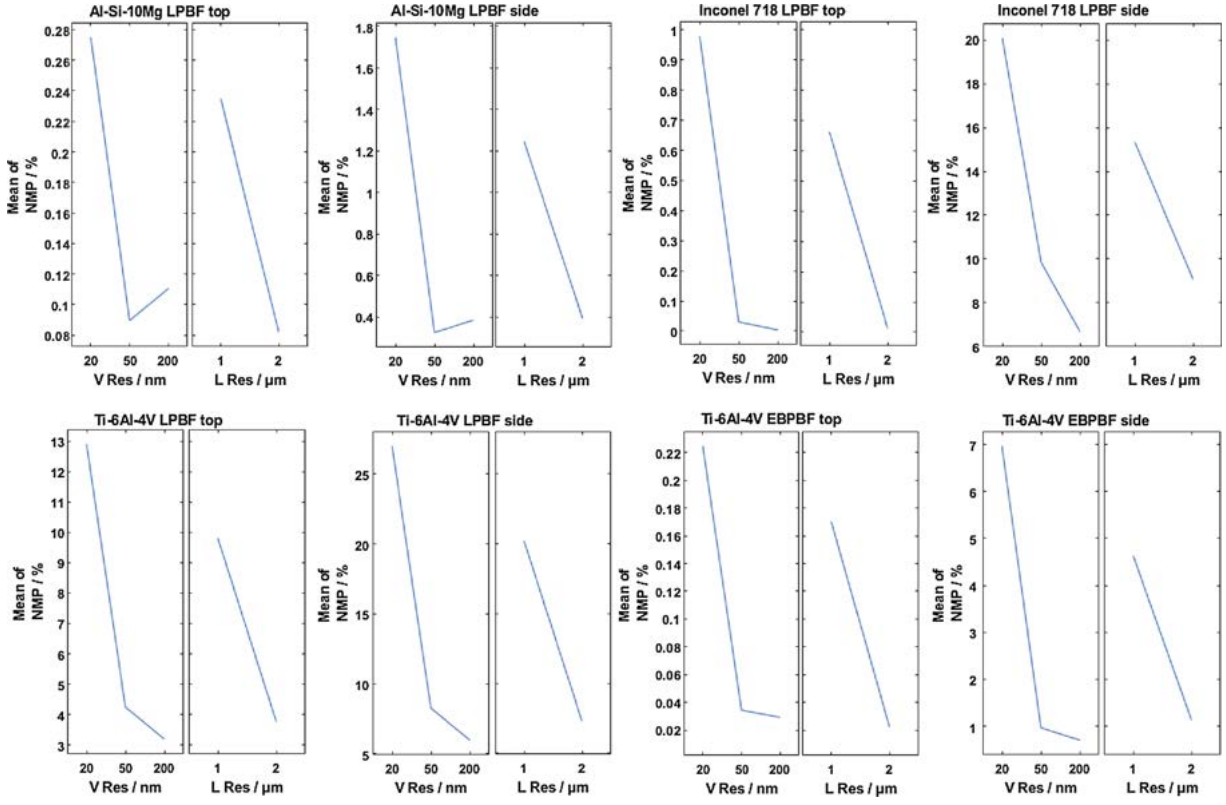

Fig. 14. Main effect plots for NMP at 50× magnification.

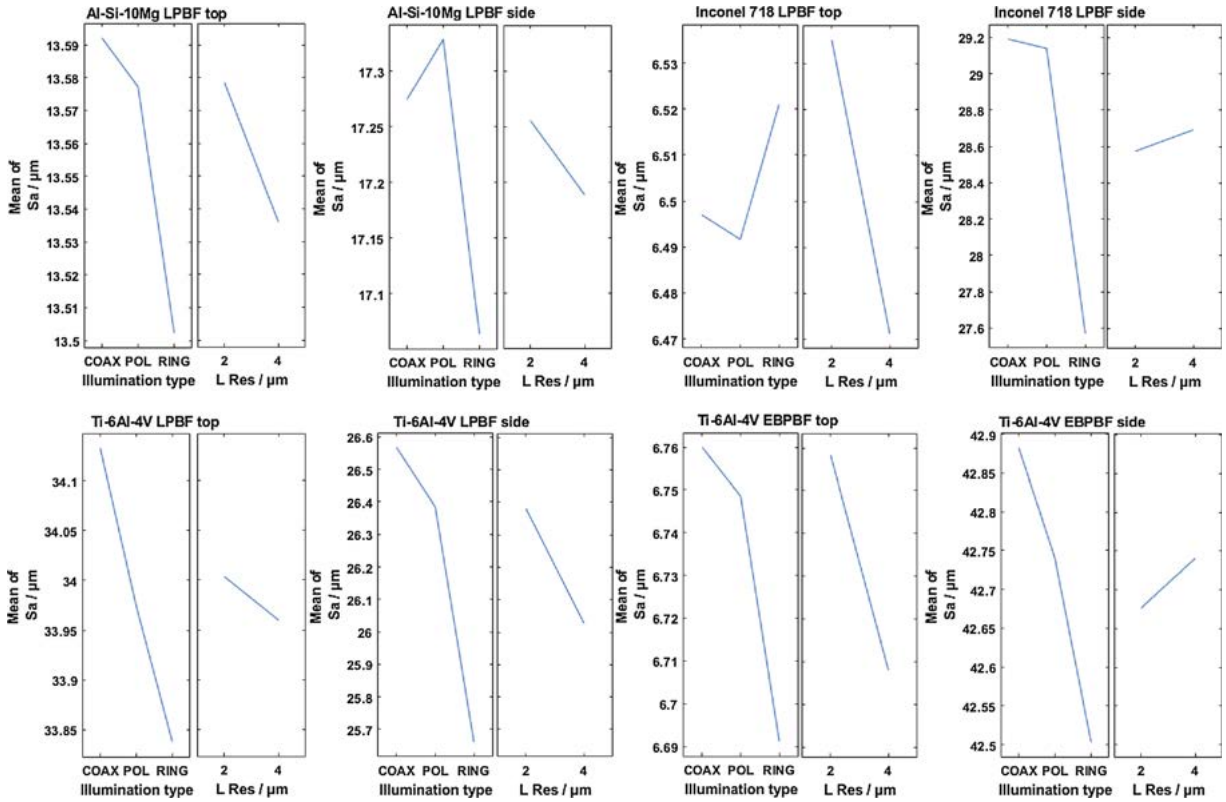

Fig. 15. Main effect plots for *Sa* at 10× magnification.

At 20× magnification (Fig. 16), only illumination type was significant. No clear trends were observed for illumination type, except that coaxial illumination would frequently lead to higher *Sa* values and ring light leading to lower *Sa*, in any case down to a fraction of a micrometre.

At 50× magnification (Fig. 17), only illumination type was significant for all cases, as seen at 20× magnification. Inconsistent trends were observed with illumination type, with coaxial frequently leading to lower *Sa* values and ring light frequently leading to higher *Sa* values, nevertheless, in most cases the parameter still only varies within a micrometre of the average value for that surface.

3.2.3.3. Summary. For *Sa*, the quality of model fitting was acceptable/good in almost all cases. Lateral resolution and illumination type were found to be significant, albeit generally resulting in inconsistent trends. Lower lateral resolution often (but not always) led to slight decreases of *Sa*, whilst effects of illumination type were found dependent on the surface. For all cases, both illumination type and lateral resolution induced variations of *Sa* that were found within a micrometre, usually one or two orders of magnitude smaller than the actual *Sa* values.

3.2.4. Summary of the results

Looking at the FV performance in computing texture parameters that summarise height properties, the FV measurement appears relatively stable with variations in the parameter value *Sa* for any surface and objective within 5% of the average value, often within a micrometre.

Concerning the actual quality of measured topography height values, measured by local repeatability error as computed by the instrument itself, then vertical resolution appears as the most significant factor. Finally, the number of non-measured points was found to associate most generally to the lateral resolution as a significant factor for all objectives. The algorithm used by the FV instrument to tag a point as non-measured are proprietary, but the assessment of local repeatability error (previous indicator) is involved, possibly through a non-linear interaction which is difficult to capture by linear regression modelling.

Regarding the measurement control parameters themselves, the following general trends can be extracted.

Vertical resolution: vertical resolution was always significant ($p < 0.05$) for Q3, with higher resolutions leading to lower Q3 values as shown in Figs. 9–11. Lower vertical resolutions consistently led to higher Q3 values, indicating on average a larger repeatability error. A possible interpretation of this, with reference to Fig. 1, is that if the instrument has fewer focal planes to consider (fewer images in the vertical stack), it may have fewer chances to find the maximum contrast point in the images available in the vertical stack and may need to rely more on interpolation. However, higher vertical resolutions also led to higher NMP at higher magnifications (at 20× and 50×), as seen in Figs. 13 and 14. Finally, from the ANOVA there was not enough evidence to confirm the influence of vertical resolution on *Sa*.

Lateral resolution: higher lateral resolutions generally led to higher NMP. This can be explained by assuming that lower lateral resolution imply the use of larger windows to compute contrast (see Fig. 1), and thus lower probability of contrast computation being inconclusive. There was not enough evidence from the ANOVA to confirm the influence of lateral resolution on Q3. Lower resolutions also usually led to smaller *Sa* values as it is considered that lower resolution acts as a low-pass filter, i.e. introducing a smoothing effect in the reconstructed topography (as shown in Fig. 7). In a few cases (some side surfaces at higher magnifications, as shown in Appendix A), the trend was inverted, presumably because of *Sa* being influenced by individual topography features (over the small measurement area) covering a higher percentage of the field of view.

Illumination type: the ANOVA was inconclusive regarding the effects of illumination type on Q3 and NMP, except at 10×

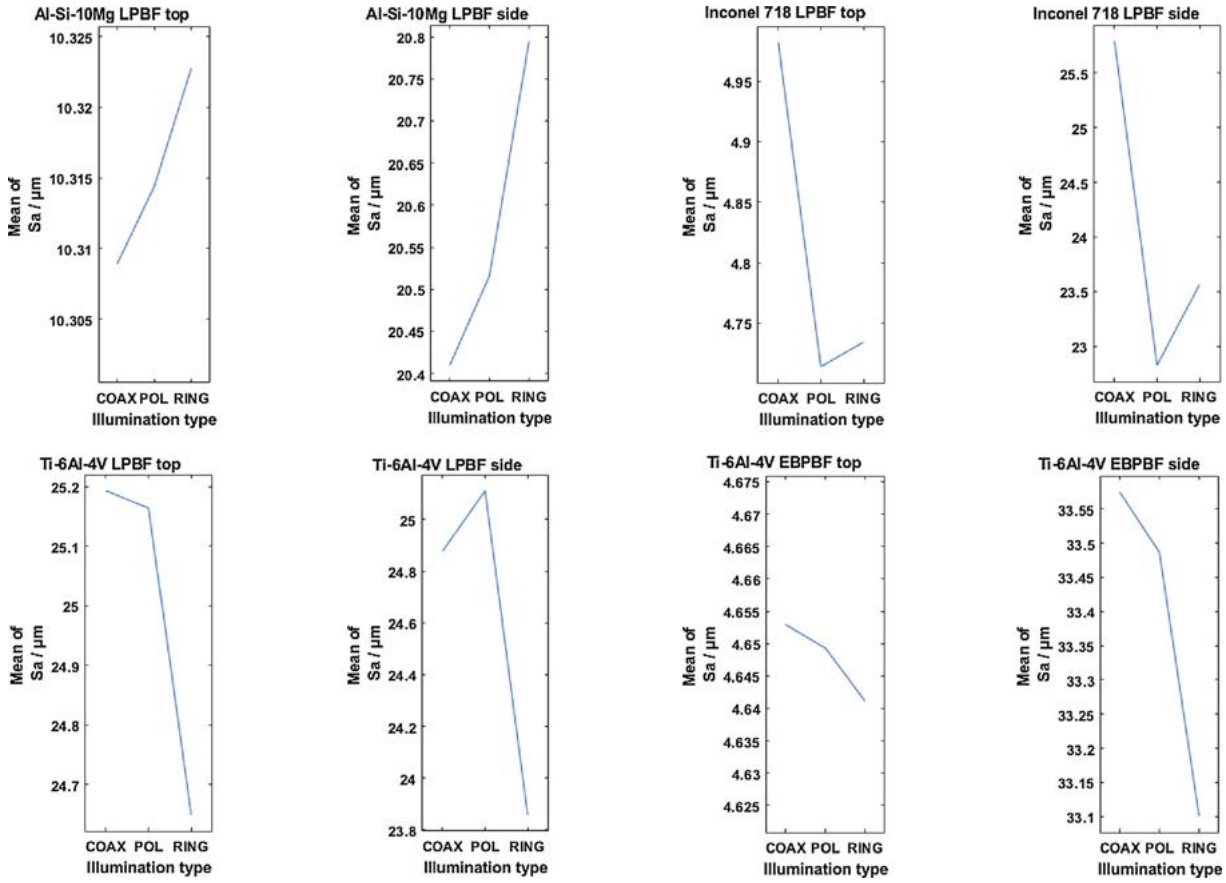

Fig. 16. Main effect plots for *Sa* at 20× magnification.

magnification, where usually smoother surfaces (top surfaces) benefitted more from ring light illumination (lower NMP). The influence of illumination type on the *Sa* parameter was consistently observed. Usually, ring light illumination led to lower *Sa* at lower magnifications (10×, 20×), as shown in Figs. 15 and 16. A not-so-consistent but inverted trend was observed at 50×, possibly because of individual features occupying a significant percentage of the field of view.

4. Discussion

4.1. General assumptions from the results

A natural question that arises after conducting an experimental study focused on a specific set of samples is can the results be generalised to different scenarios (different materials, manufacturing processes, surface geometries). Although this work only considered metal additive surfaces, concentrating solely on powder bed fusion technologies, it is apparent that a wide array of surface topographies was still generated, because of the variability arising from the exploration of multiple combinations of manufacturing processes, materials and surface orientations. Within this work, surface topographies ranging from smooth to rough, from highly reflective to poorly reflective, from low to high aspect-ratio were covered. It is, therefore, reasonable to assume that surfaces originating from different manufacturing processes, but ultimately similar in terms of topographic complexity and possibly optical properties, may lead to similar behaviour with FV technology.

4.2. The meaning of measurement quality

In the majority of cases pertaining to the characterisation of surface topography in industrial scenarios, the role of surface measurement is to produce an assessment of “roughness” quantified in terms of texture parameters, such as the *Sa* parameter from the ISO 25178-2 standard, which was evaluated in this work. If the role of surface metrology is to compute texture parameters, then it was shown how results were relatively similar across different FV measurement set-ups (though the area size was below those recommended in the standard). This is mostly because of the averaging effects of texture parameters such as *Sa*, where local discrepancies between topographic reconstructions are easily absorbed in the computation of summary indicators that apply to the entire measured field [34]. However, when considering the accuracy of the actual individual, reconstructed topographic features, then more detailed investigations are needed. An indicator such as NMP (percentage of non-measured points), which was used in this work, only provides information about whether the instrument deemed the acquired raw information reliable enough to produce a point height estimate, which may not necessarily mean that the measurement is correct. Analogously, an indicator such as Q3 (upper quartile of repeatability error), which was also used in this work, only indicates the instrument’s own assessment of repeatability, which again does not consider the possibility of local bias, and thus lack of accuracy, in the measurement.

Previous work on the generation of statistical topography models from repeated measurements [9,15] shows that more comprehensive assessment of measurement quality, intended as true metrological performance

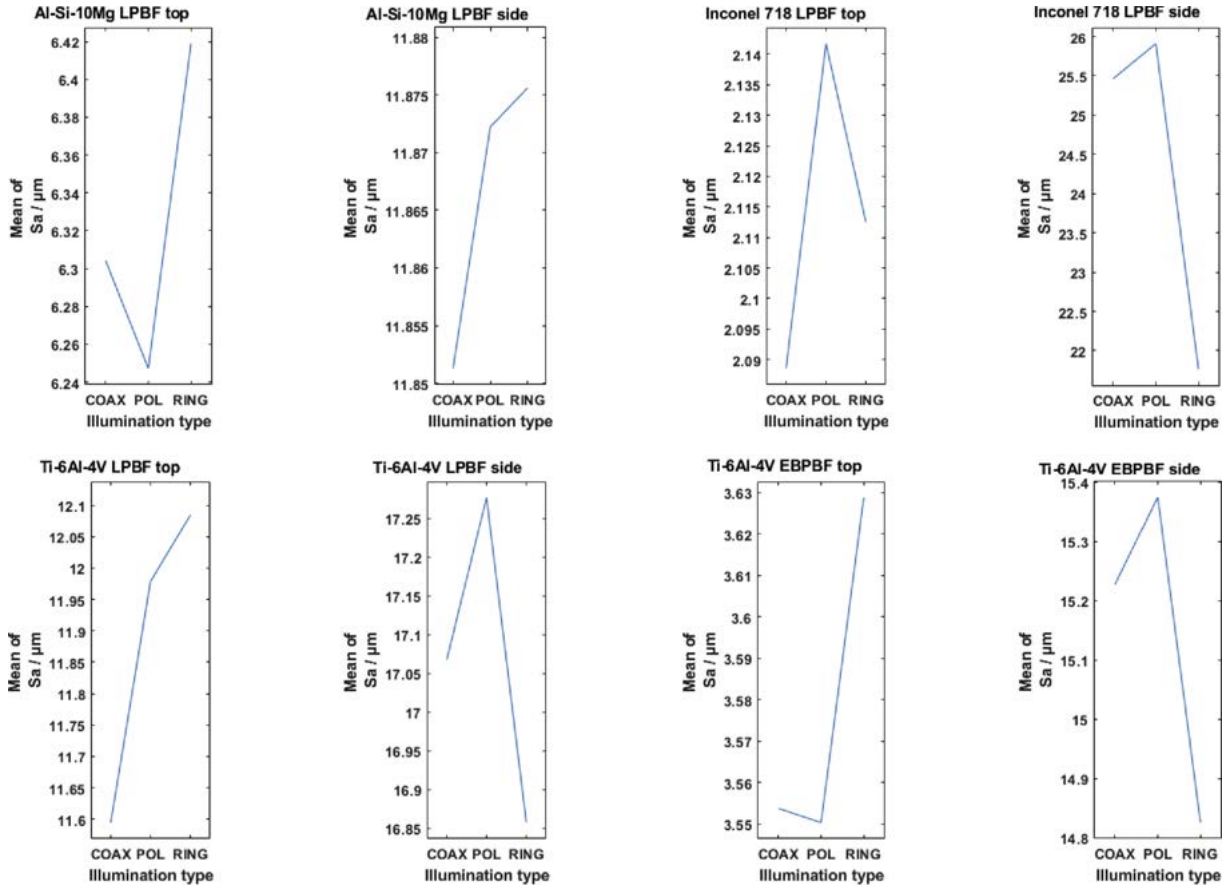

Fig. 17. Main effect plots for *Sa* at 50× magnification.

and thus useable to obtain an uncertainty estimate, may be possible as long as a more accurate measurement result (traceable) is available to act as reference. However, such comparison is at the moment missing for the experimental campaign carried out in this study, and the challenge of understanding how uncertainty should be computed and associated to surface topography characterisation is currently unsolved [35].

In summary, it is possible to say that values of parameters such as *Sa* are relatively consistent across measurement set-ups, but it is not possible to say whether the metrological quality of the reconstructed topographies (in particular in terms of accuracy) is better or worse in some set-ups versus others. This is because neither NMP nor Q3 are suitable indicators for accuracy, as comparison with a more accurate reference and appropriate, supporting statistical models is needed.

4.3. General advice on FV configuration for the measurement of metal additive surfaces

As the results have hopefully shown, there is no such thing as a 'metal additive surface'. When looking at powder bed fusion methods, if the material, orientation, or process (laser vs electron beam) is changed, different surfaces will be generated, each one with different topography and optical properties, thus presenting different challenges for FV measurement. However, a few general indications for the measurement control parameters: vertical resolution, lateral resolution, and illumination type can be provided for someone performing a measurement of a metal additive surface with a FV instrument.

Vertical resolution should be balanced to improve the repeatability error of the measurement whilst not leading to too many non-measured points. It was observed that whilst improved vertical resolutions lead to lower Q3 it also increased NMP. Top surfaces generally possess lower NMP from measurement, so it can be suggested that improved vertical resolutions may be used when measuring top surfaces. Side surfaces however typically result in higher NMPs, likely because of hard-to-measure features of the surface, such as particles. For side surfaces, the use of lower vertical resolutions may be suggested, as it would allow for a reduction in NMP. This would likely come at the cost of quality (Q3, repeatability error) and lower *Sa*, so a trade-off may be sought, depending on application needs.

Lateral resolution should be chosen based on the smallest scale that is of interest to capture in the measurement. However, the user ought to use the lowest resolutions that can still capture the features of interest, as it was observed that lower lateral resolutions lead to lower NMP and, in case of lower magnifications, also lower *Sa*. As observed by visual inspection (Fig. 7), lateral resolution influences the smallest scale of spatial frequencies that are captured on the surface, therefore it is important to ensure that this smoothing effect of worse resolution is kept to a minimum whilst insuring good coverage in the measurement of the surface.

Illumination type should be chosen based on the type of surface, material and orientation and the ability to adequately illuminate the surface without causing issues with contrast in the image (under- or over-exposure), which can be seen in Fig. 8. Higher NMP were observed with coaxial and lower NMP with ring illumination for top surfaces, whilst the opposite was observed for side surfaces suggesting that coaxial light can

capture aspects of the side surface better than ring light.

Ultimately, regardless of measurement setup, texture parameters such as *Sa* are not going to be affected that much by changing measurement process parameters. Observed variations for *Sa* were confined to 5% (typically within one micrometre range) of the average for that measured. However, when considering the accuracy of the actual detail of the reconstruction of the measured topography as opposed to surface texture parameters, then the above findings should be considered with additional care.

It is important to point out that this work presents results addressing flat surfaces only, as the measurement of curved surfaces present additional challenges that reflect the limitations of current state-of-the-art topography measurement systems in acquiring topography at high resolutions whilst simultaneously guaranteeing large lateral and vertical ranges. Whilst it is believed that, locally, the performance and behaviour of FV measurement should reflect what observed in this work as the main instrument control parameters are changed, large scale investigations of arbitrarily curved surfaces are likely to introduce additional challenges deserving a more comprehensive investigation. Most instruments nowadays resort to stitching, a technology where multiple measured datasets are collated in space in order to extend the spatial coverage of the measurement. However, stitching, like any other data processing method, introduces further sources of error which have not been covered in this paper.

A final comment should be reserved to comparing the ISO 25178-2 *Sa* texture parameter values obtained via FV and discussed throughout the paper, to the ISO 4287 *Ra* roughness parameter values obtained via stylus measurements and reported for reference in Table 2. Despite *Sa* and *Ra* having basically identical mathematical definitions (both are the arithmetic mean vertical distance of surface/profile points a best-fit mean reference geometry - plane/line), the two parameters cannot be directly compared from a strict, numerical standpoint. Firstly, because *Sa* and *Ra* are representative of a differently sampled surface: *Ra* being computed only on a few profiles, *Sa* being computed over a more comprehensive, areal sampling. Secondly because levelling work differently on profile and areal data: each profile is independently levelled by subtraction of the best-fit mean line, whilst areal data is levelled all at once with a single best-fit mean plane. Thirdly, because filtering and filter cut-off choices were differently set in this work for *Sa* and *Ra*.

Despite the *Ra* and *Sa* values reported in this manuscript not exactly corresponding to each other, it is important to highlight the fact that the trends observed for *Sa* obtained via FV measurement (i.e. which surfaces are rougher than whom) do correspond to the trends seen for *Ra* obtained via stylus. This is irrespective of set-up of the optical instrument and provides a comforting indication that a general assessment of roughness can be obtained via FV measurement, even with a sub-optimal setup.

5. Conclusions

This work explored focus variation (FV) measurement of metal additive surfaces. The sensitivity of FV measurement to control parameters which are commonly set during the measurement, specifically magnification, vertical resolution, lateral resolution and illumination type, was studied as FV measurement was applied to surfaces of additive parts fabricated with aluminium alloy Al-Si-10Mg; nickel super alloy Inconel 718; and titanium alloy Ti-6Al-4V, produced by laser powder bed fusion or electron beam powder bed fusion, and oriented horizontally or vertically with respect to the build direction.

The results indicate that there is a wide array of surface topographies and optical properties represented by metal additive surfaces. Despite the variability, some general conclusions can be drawn by building regression models on full factorial design of experiments. In particular, the computation of surface texture parameters such as *Sa* (ISO 25178-2 [31]) are mostly unaffected by the various set-ups explored, and always consistent with the trends observed via the more industrially accepted stylus-based measurement and computation of the *Ra* parameter. However, other indicators such as local repeatability error in height determination and the percentage of non-measured points are significantly affected by the control parameters, albeit the magnitude of such effects, and the generated trends, may vary with surface type. The contribution of this work is a method for sensitivity analysis based on regression modelling, useful for exploring the behaviour of any measurement instrument when applied to a wide range of measured surfaces. Finally, this work once more highlights the underlying, currently unsolved challenge of understanding how uncertainty should be computed and associated to surface topography data.

Although this work provides useful guidelines for AM users to improve the quality of their FV measurement results, a more thorough investigation is needed to understand specifically what topographic properties (local slope, aspect ratio, optical properties, etc.) affect FV behaviour and performance and to what extent. This is likely to imply a more extensive experimentation based on artificial surfaces and systematic testing of combinations. Another challenge is to properly unravel the internal mechanism of the specific FV instrument which may prove hard because of understandable needs for IP protection, but is nevertheless necessary for a fuller understanding of how the measurement control parameters affect actual performance. Finally, a proper assessment of FV measurement performance should include a connection to a more accurate reference which allows the investigation of trueness and traceability.

Acknowledgments

We would like to thank the Engineering and Physical Sciences Research Council (Grants EP/L01534X/1 and EP/M008983/1) and the Manufacturing Technology Centre (Coventry, UK) for funding this work. We would also like to thank Bethan Smith of the Manufacturing Technology Centre (Coventry, UK) and Adam Thompson of the Manufacturing Metrology Team and Centre for Additive Manufacturing (Nottingham, UK) for providing the samples.

Appendix A. Full ANOVA Results

Coefficient of determination (R^2) results.
See Tables A1–A3.

Table A1
Coefficient of determination (R^2) results for the 10× objective ANOVA models.

10× magnification			
Surface	R^2 values		
	Q3/nm	NMP / %	Sa/μm
Al-Si-10Mg LPBF Top	0.989	0.971	0.993
Al-Si-10Mg LPBF Side	0.990	0.731	0.995
Inconel 718 LPBF Top	0.715	0.987	0.981
Inconel 718 LPBF Side	0.997	0.867	0.992
Ti-6Al-4V LPBF Top	0.873	0.899	0.986
Ti-6Al-4V LPBF Side	0.993	0.840	0.997
Ti-6Al-4V EBPBF Top	0.985	0.931	0.980
Ti-6Al-4V EBPBF Side	0.996	0.806	0.997

Table A2
Coefficient of determination (R^2) results for the 20× objective ANOVA models.

20× magnification			
Surface	R^2 values		
	Q3/nm	NMP / %	Sa/μm
Al-Si-10Mg LPBF Top	0.979	0.556	0.761
Al-Si-10Mg LPBF Side	0.978	0.663	0.827
Inconel 718 LPBF Top	0.763	0.649	0.999
Inconel 718 LPBF Side	0.969	0.841	0.948
Ti-6Al-4V LPBF Top	0.943	0.776	0.865
Ti-6Al-4V LPBF Side	0.941	0.761	0.924
Ti-6Al-4V EBPBF Top	0.939	0.574	0.978
Ti-6Al-4V EBPBF Side	0.911	0.758	0.925

Table A3
Coefficient of determination (R^2) results for the 50× objective ANOVA models.

50× magnification			
Surface	R^2 values		
	Q3/nm	NMP/%	Sa/μm
Al-Si-10Mg LPBF Top	0.989	0.768	0.967
Al-Si-10Mg LPBF Side	0.975	0.750	0.805
Inconel 718 LPBF Top	0.920	0.775	0.988
Inconel 718 LPBF Side	0.829	0.787	0.979
Ti-6Al-4V LPBF Top	0.608	0.813	0.966
Ti-6Al-4V LPBF Side	0.998	0.906	0.829
Ti-6Al-4V EBPBF Top	0.989	0.727	0.994
Ti-6Al-4V EBPBF Side	0.984	0.825	0.977

See Figs. A1–A9.

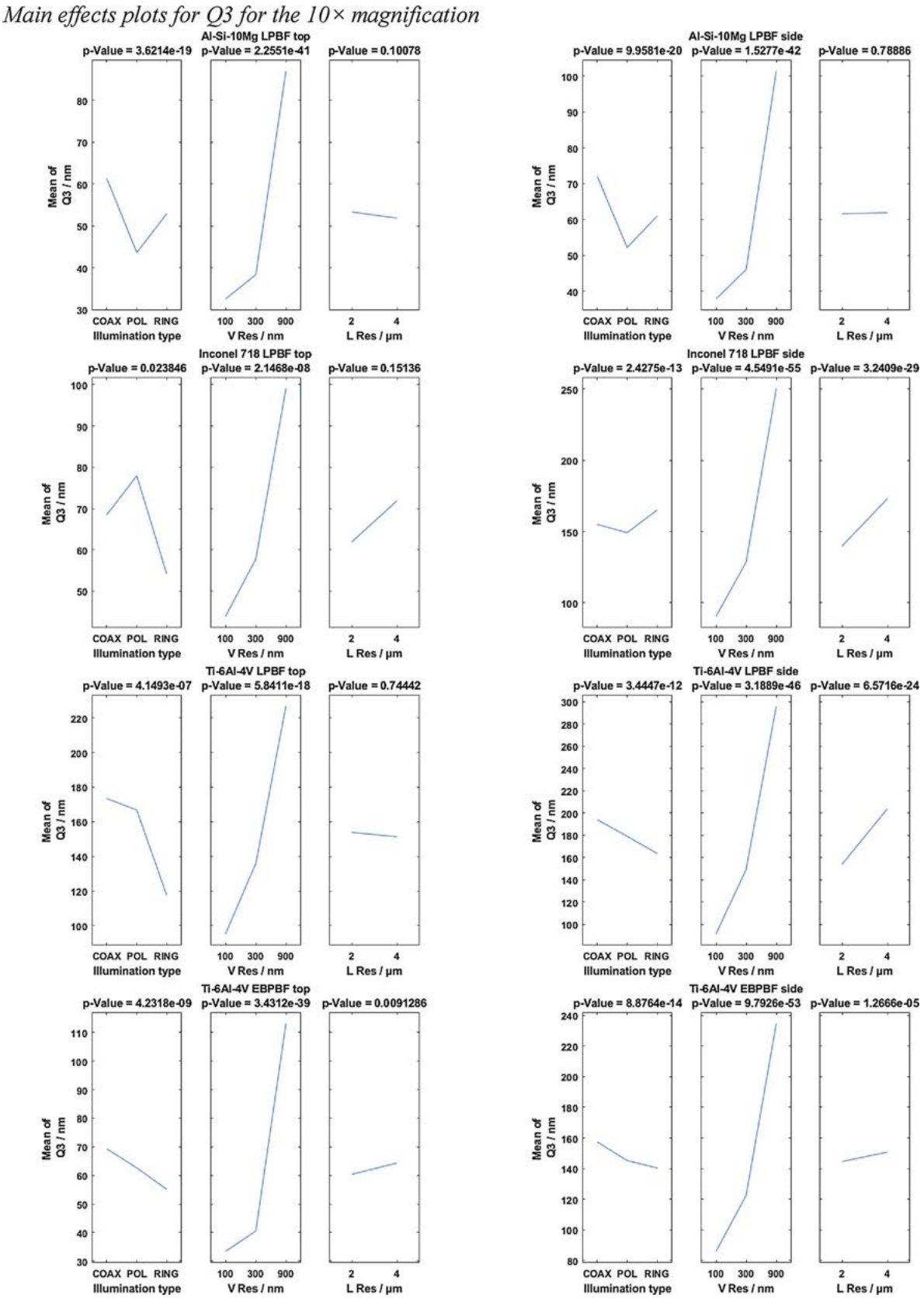

Fig. A1. Main effects plots for Q3 for the 10× magnification.

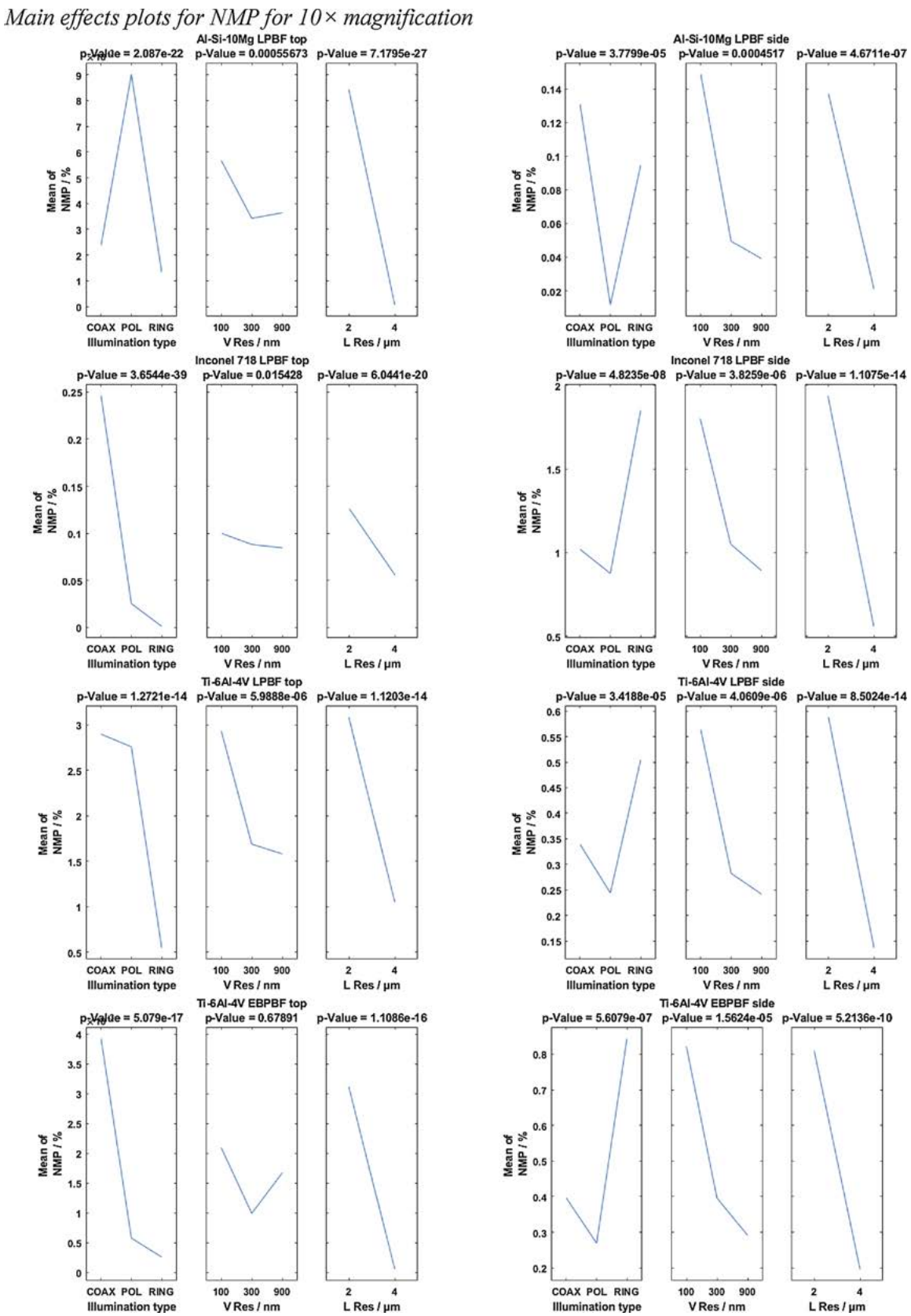

Fig. A2. Main effects plots for NMP for the 10× magnification.

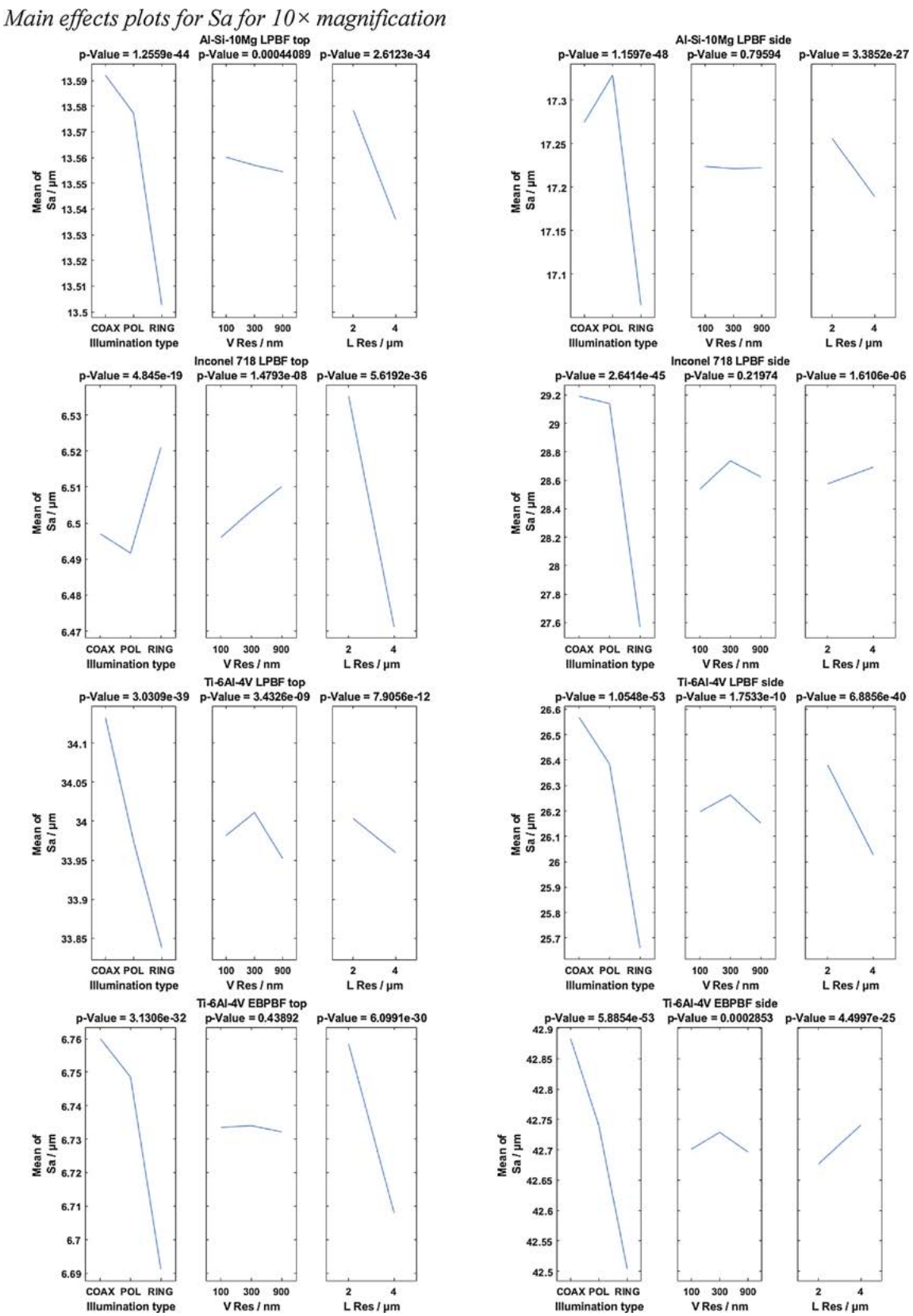

Fig. A3. Main effects plots for *Sa* for the 10× magnification.

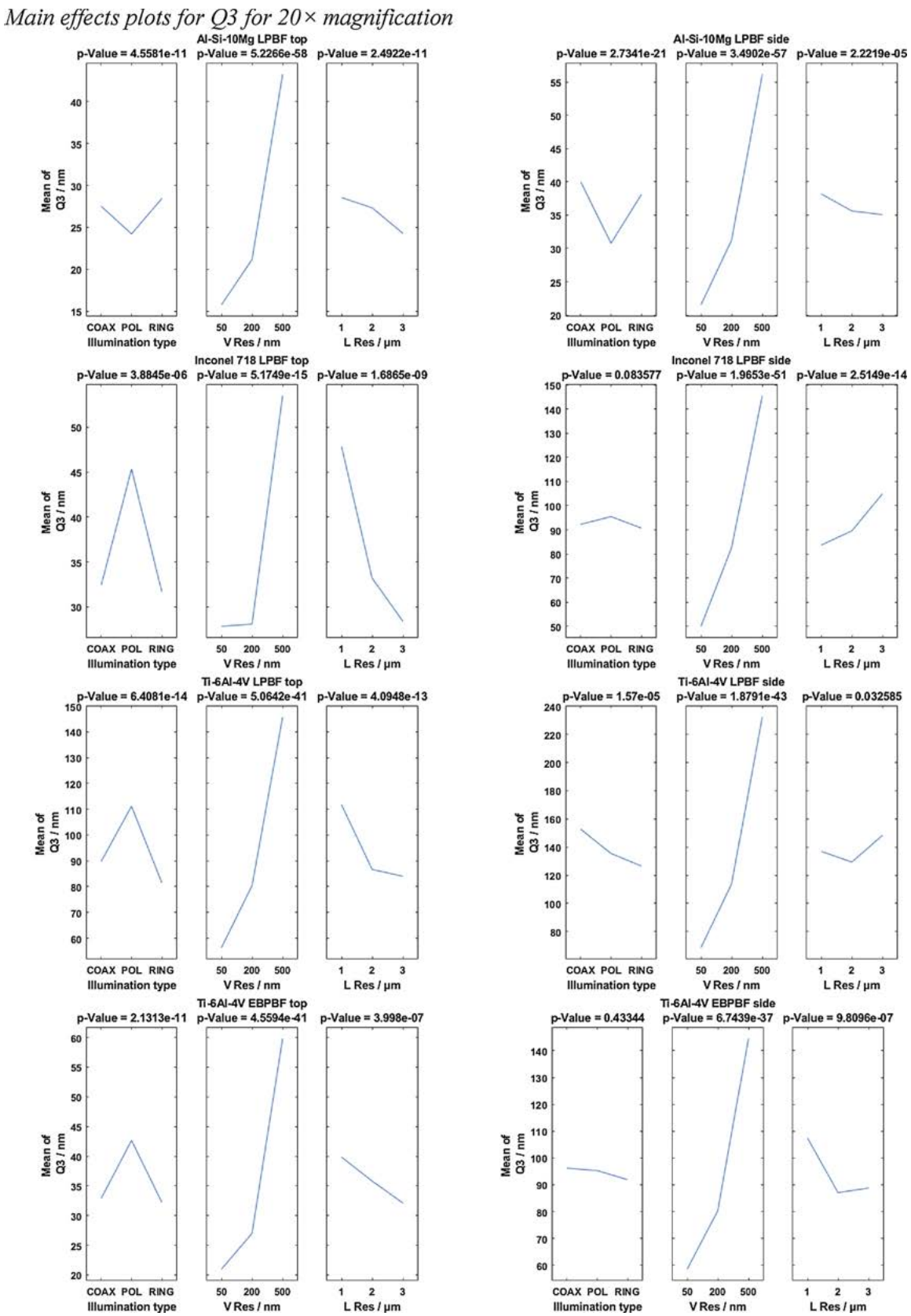

Fig. A4. Main effects plots for Q3 for the 20× magnification.

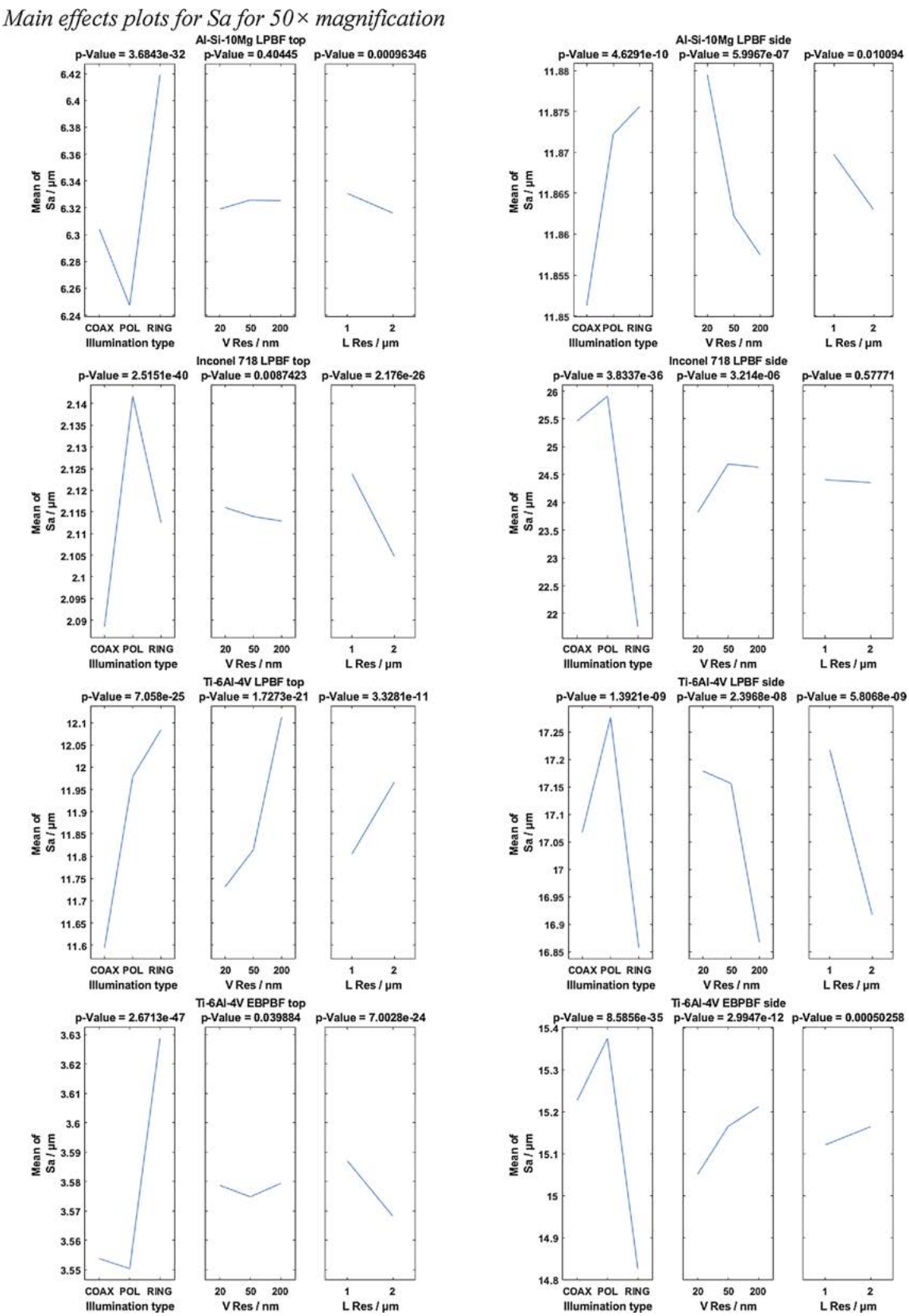

Fig. A5. Main effects plots for NMP for the 20× magnification.

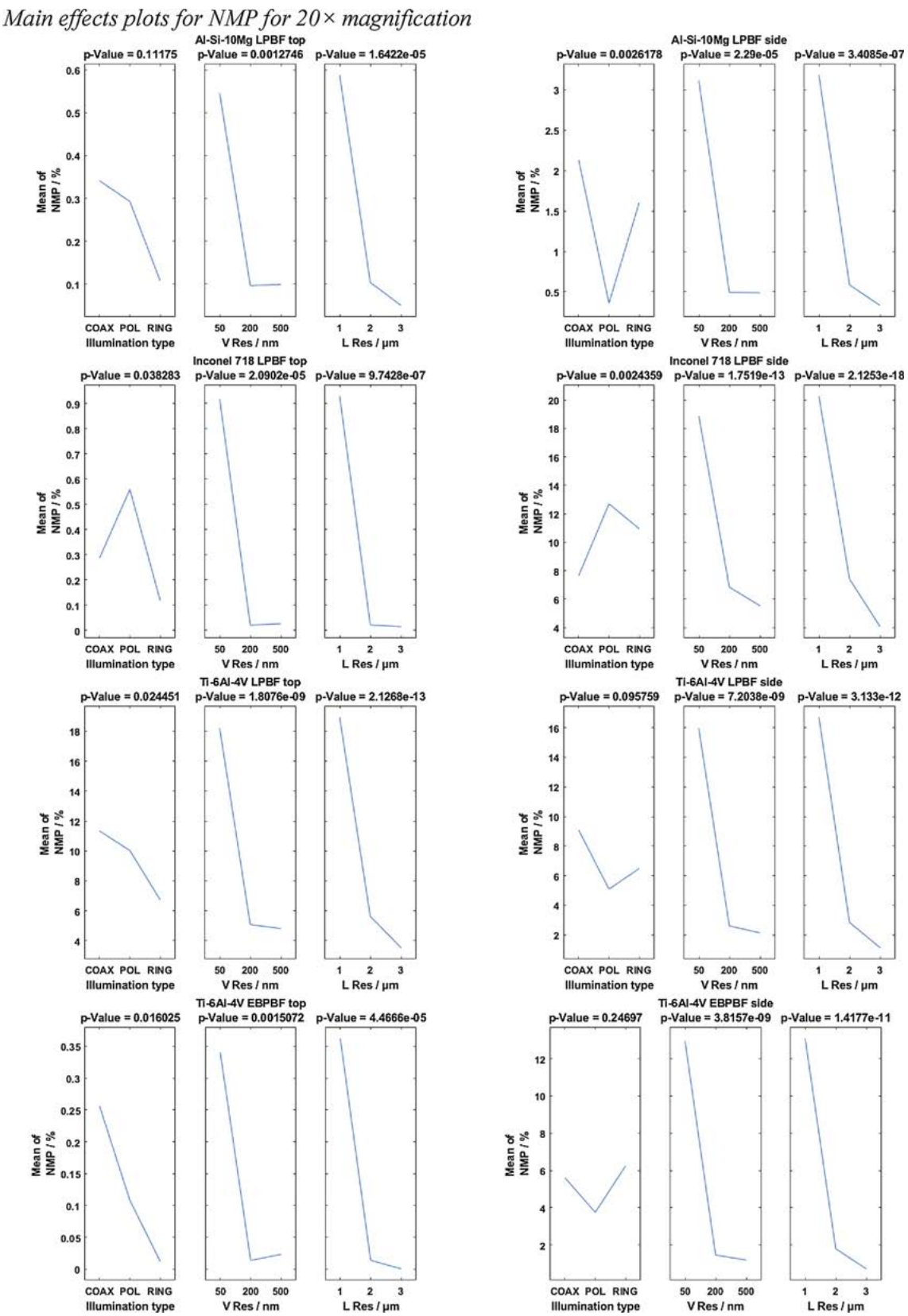

Fig. A6. Main effects plots for *Sa* for the 20× magnification.

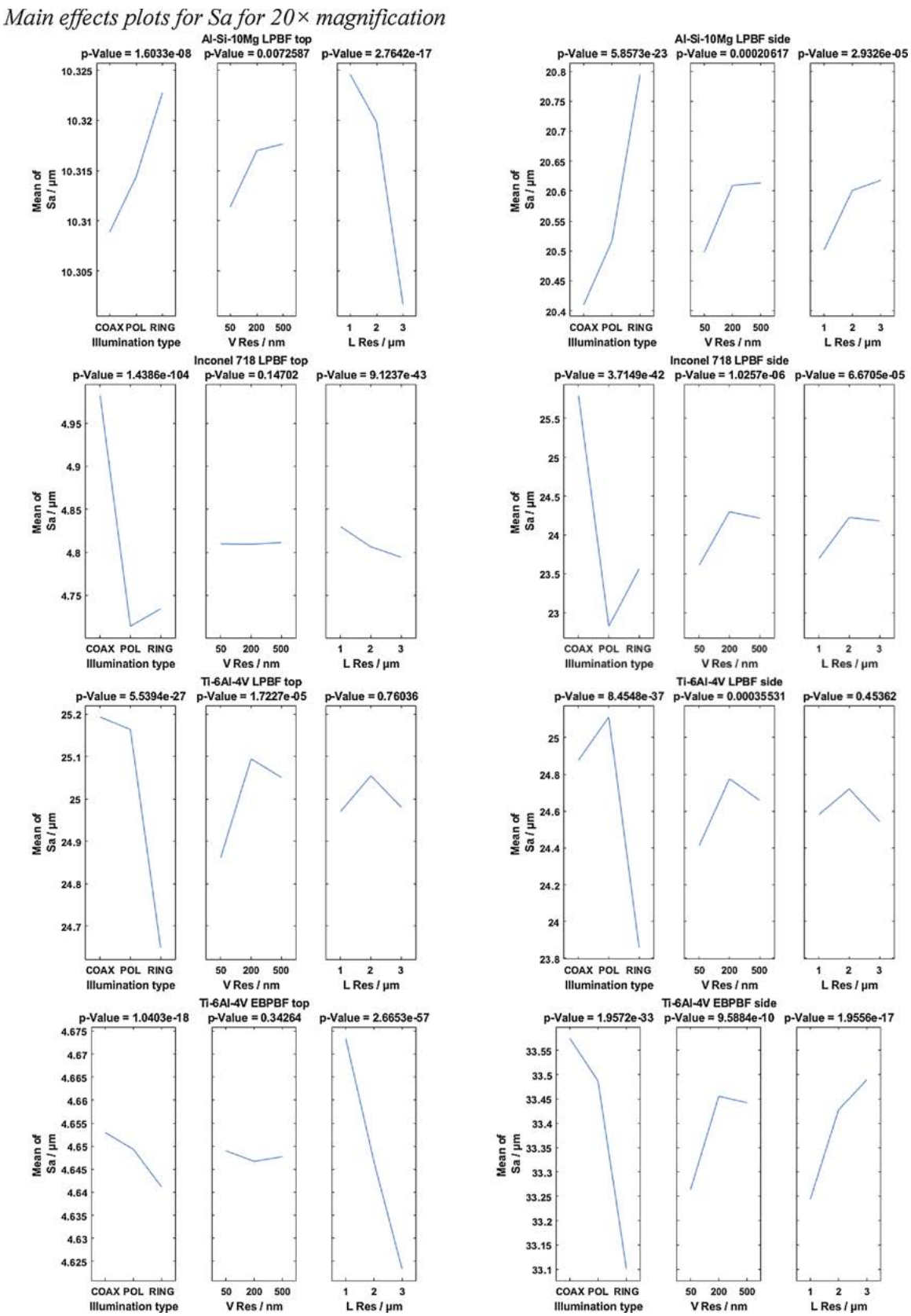

Fig. A7. Main effects plots for Q3 for the 50× magnification.

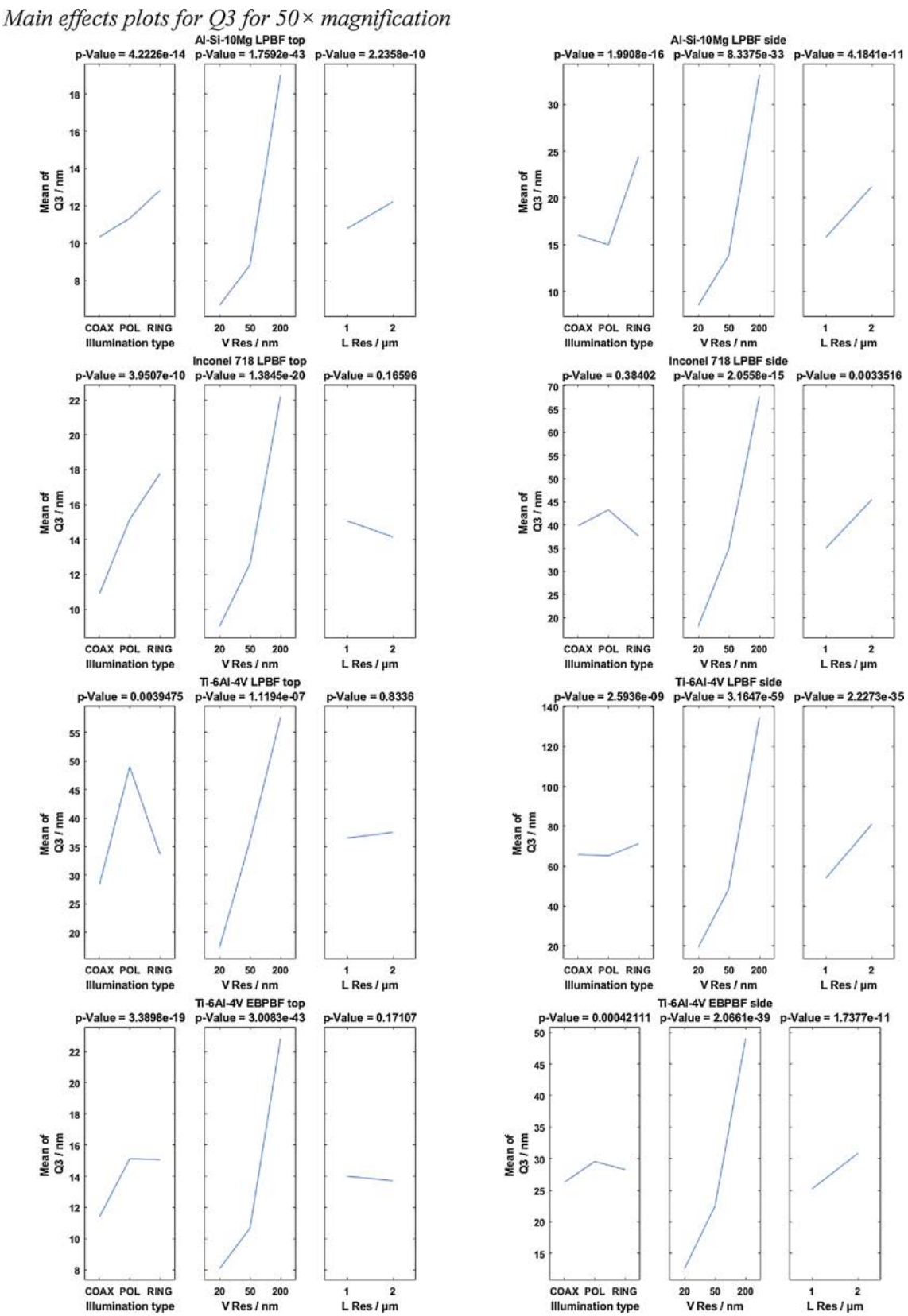

Fig. A8. Main effects plots for NMP for the 50× magnification.

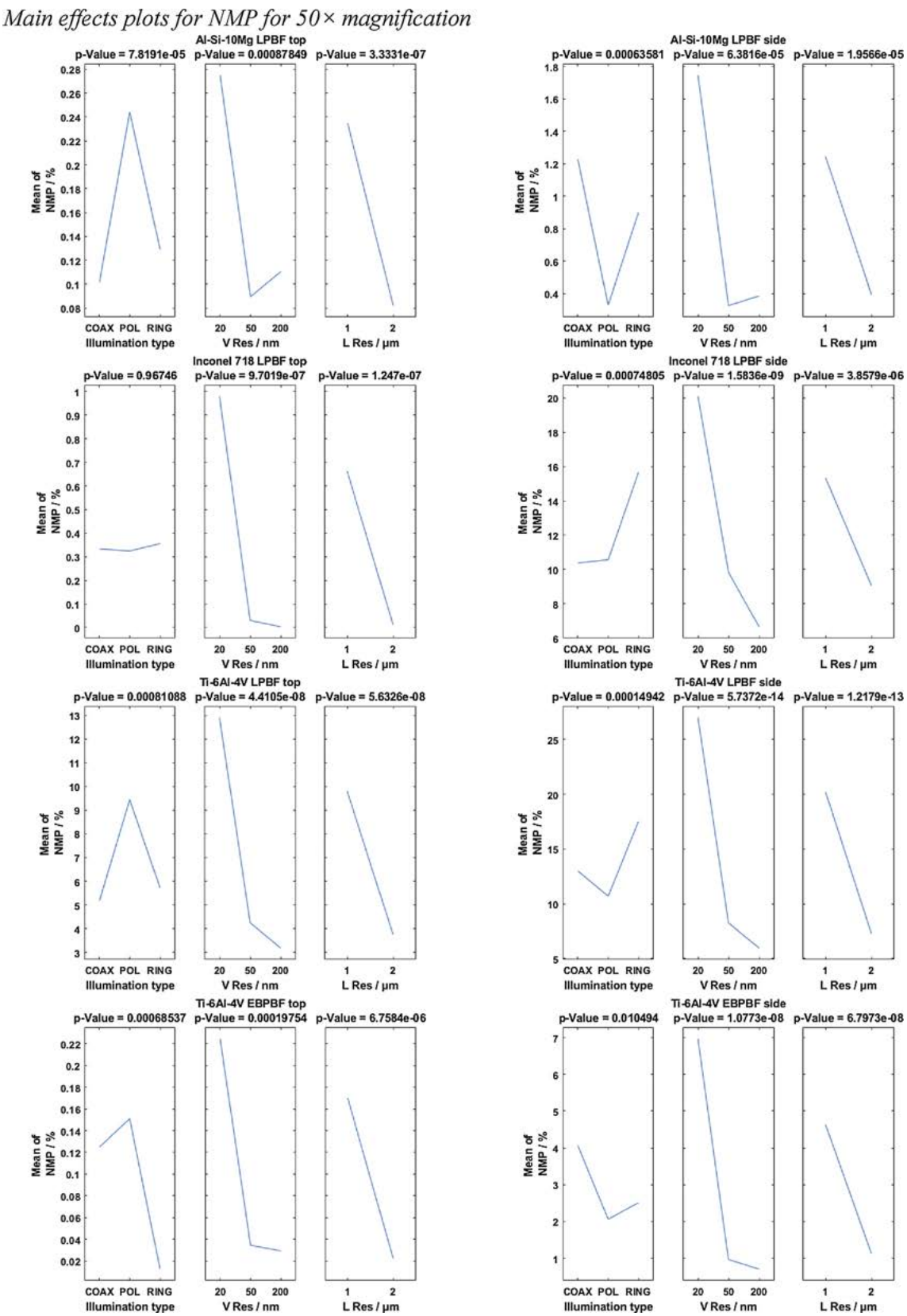

Fig. A9. Main effects plots for *Sa* for the 50× magnification.

References

[1] I. Gibson, D. Rosen, B. Stucker, Design for additive manufacturing, Addit. Manuf. Technol. 3D Printing, Rapid Prototyping, Direct Digit. Manuf. 2nd ed., Springer New York, New York, USA, 2014 pp. 399–343.

[2] ISO, ISO 17296-2 - Additive Manufacturing—General Principles Part 2: Overview of Process Categories and Feedstock, (2016).

[3] L.E. Murr, S.M. Gaytan, D.A. Ramirez, E. Martinez, J. Hernandez, K.N. Amato, P.W. Shindo, F.R. Medina, R.B. Wicker, Metal fabrication by additive manufacturing using laser and electron beam melting technologies, J. Mater. Sci. Technol. 28 (2012) 1–14, https://doi.org/10.1016/S1005-0302(12)60016-4.

[4] F. Calignano, D. Manfredi, E.P. Ambrosio, L. Iuliano, P. Fino, Influence of process parameters on surface roughness of aluminum parts produced by DMLS, Int. J. Adv. Manuf. Technol. 67 (2013) 2743–2751, https://doi.org/10.1007/s00170-012-4688-9.

[5] A. Triantaphyllou, C.L. Giusca, G.D. Macaulay, F. Roerig, M. Hoebel, R.K. Leach, B. Tomita, K.A. Milne, Surface texture measurement for additive manufacturing, Surf. Topogr. Metrol. Prop. 3 (2015), https://doi.org/10.1088/2051-672X/3/2/024002.

[6] T. Grimm, G. Wiora, G. Witt, Characterization of typical surface effects in additive manufacturing with confocal microscopy, Surf. Topogr. Metrol. Prop. 3 (2015), https://doi.org/10.1088/2051-672X/3/1/014001.

[7] J.C. Fox, S.P. Moylan, B.M. Lane, Effect of process parameters on the surface roughness of overhanging structures in laser powder bed fusion additive manufacturing, Procedia CIRP 45 (2016) 131–134, https://doi.org/10.1016/j.procir.2016.02.347.

[8] Z. Chen, X. Wu, D. Tomus, C.H.J. Davies, Surface roughness of selective laser melted Ti-6Al-4V alloy components, Addit. Manuf. 21 (2018) 91–103, https://doi.org/10.1016/j.addma.2018.02.009.

[9] A. Thompson, N. Senin, C. Giusca, R. Leach, Topography of selectively laser melted surfaces: a comparison of different measurement methods, CIRP Ann. Manuf. Technol. 66 (2017) 543–546, https://doi.org/10.1016/j.cirp.2017.04.075.

[10] N. Senin, A. Thompson, R.K. Leach, Characterisation of the topography of metal additive surface features with different measurement technologies, Meas. Sci. Technol. 28 (2017) 095003, , https://doi.org/10.1088/1361-6501/aa7ce2.

[11] N. Senin, A. Thompson, R. Leach, Feature-based characterisation of signature topography in laser powder bed fusion of metals, Meas. Sci. Technol. 29 (2018), https://doi.org/10.1088/1361-6501/aa9e19.

[12] A. du Plessis, S.G. le Roux, Standardized X-ray tomography testing of additively manufactured parts: A round robin test, Addit. Manuf. 24 (2018) 125–136, https://doi.org/10.1016/J.ADDMA.2018.09.014.

[13] A. Townsend, N. Senin, L. Blunt, R.K. Leach, J.S. Taylor, Surface texture metrology for metal additive manufacturing: a review, Precis. Eng. 46 (2016) 34–47, https://doi.org/10.1016/j.precisioneng.2016.06.001.

[14] C. Gomez, R. Su, A. Thompson, J. DiSciacca, S. Lawes, R. Leach, Optimization of surface measurement for metal additive manufacturing using coherence scanning interferometry, Opt. Eng. 56 (2017) 111714, , https://doi.org/10.1117/1.OE.56.11.111714.

[15] N. Senin, A. Thompson, R.K. Leach, Characterisation of the topography of metal additive surface features with different measurement technologies, Meas. Sci. Technol. 28 (2017), https://doi.org/10.1088/1361-6501/aa7ce2.

[16] J.P. Kruth, P. Mercelis, J. Van Vaerenbergh, L. Froyen, M. Rombouts, Binding mechanisms in selective laser sintering and selective laser melting, Rapid Prototyp. J. 11 (2005) 26–36, https://doi.org/10.1108/13552540510573365.

[17] C. Körner, Additive manufacturing of metallic components by selective electron beam melting—a review, Int. Mater. Rev. 61 (2016) 361–377, https://doi.org/10.1080/09506608.2016.1176289.

[18] F. Helmli, Focus variations instruments, in: R.K. Leach (Ed.), Opt. Meas. Surf. Topogr. Springer, Berlin Heidelberg, 2013, , https://doi.org/10.1007/978-3-642-12012-1.

[19] R. Danzl, F. Helmli, S. Scherer, Focus variation–a robust technology for high resolution optical 3D surface metrology, Stroj. Vestnik/J. Mech. Eng. 57 (2011) 245–256, https://doi.org/10.5545/sv-jme.2010.175.

[20] ISO, ISO 25178-607 (GPS)—Surface Texture: Areal—Part 607: Nominal Characteristics of non-Contact (Confocal Microscopy) Instruments, (2017).

[21] F. Cabanettes, A. Joubert, G. Chardon, V. Dumas, J. Rech, C. Grosjean, Z. Dimkovski, Topography of as built surfaces generated in metal additive manufacturing: a multi scale analysis from form to roughness, Precis. Eng. 52 (2018) 249–265, https://doi.org/10.1016/j.precisioneng.2018.01.002.

[22] A. Townsend, R. Racasan, L. Blunt, Surface-Specific Additive Manufacturing Test Artefacts, (2018), https://doi.org/10.1088/2051-672X/aabcaf.

[23] P. Wang, W.J. Sin, M.L.S. Nai, J. Wei, Effects of processing parameters on surface roughness of additive manufactured Ti-6Al-4V via electron beam melting, Materials (Basel) 10 (2017) 8–14, https://doi.org/10.3390/ma10101121.

[24] W.S. Gora, Y. Tian, A.P. Cabo, M. Ardron, R.R.J. Maier, P. Prangnell, N.J. Weston, D.P. Hand, Enhancing surface finish of additively manufactured titanium and cobalt chrome elements using laser based finishing, Phys. Procedia 83 (2016) 258–263, https://doi.org/10.1016/j.phpro.2016.08.021.

[25] Y.Y. Sun, S. Gulizia, C.H. Oh, D. Fraser, M. Leary, Y.F. Yang, M. Qian, The influence of as-built surface conditions on mechanical properties of Ti-6Al-4V additively manufactured by selective electron beam melting, JOM 68 (2016) 791–798, https://doi.org/10.1007/s11837-015-1768-y.

[26] B. Rosa, P. Mognol, J.-Y. Hascoet, Laser polishing of additive laser manufacturing surfaces, J. Laser Appl. 27 (2015), https://doi.org/10.2351/1.4906385.

[27] A.G. Demir, B. Previtali, Additive manufacturing of cardiovascular CoCr stents by selective laser melting, Mater. Des. 119 (2017) 338–350, https://doi.org/10.1016/j.matdes.2017.01.091.

[28] N. Nikolaev, J. Petzing, J. Coupland, Focus variation microscope: linear theory and surface tilt sensitivity, Appl. Opt. 55 (2016) 3555, https://doi.org/10.1364/AO.55.003555.

[29] F. Hiersemenzel, J.D. Claverley, J.N. Petzing, R.K. Leach, F.S. Helmli, Areal surface topography measurement of high aspect ratio features using the focus variation technique, Harmnst 2013 (2013) 2–3.

[30] ISO, ISO 4287 - Geometrical Product Specification (GPS) - Surface Texture : Profile Method - Terms, Definitions and Surface Texture Parameters, (2009), https://doi.org/10.3403/02031657.

[31] ISO, Geometrical Product Specifications (GPS) - Surface Texture: Areal - Part 2: Terms, Definitions and Surface Texture Parameters, (2012).

[32] F. Blateyron, The areal field parameters, in: R.K. Leach (Ed.), Characterisation Areal Surf. Texture, Springer Berlin Heidelberg, Berlin, Heidelberg, 2013, , https://doi.org/10.1007/978-3-642-36458-7_2 pp. 15–43.

[33] Digital Surf, Mountains® surface imaging & metrology software, Digitalsurf.Com/. (2018). http://www.digitalsurf.com/en/mntkey.html.

[34] R.K. Leach, R.K. Leach (Ed.), Characterization of Areal Surface Texture, Springer Berlin Heidelberg, 2013, , https://doi.org/10.1007/978-3-642-36458-7.

[35] H. Haitjema, Uncertainty in measurement of surface topography, Surf. Topogr. Metrol. Prop. 3 (2015) 035004, , https://doi.org/10.1088/2051-672X/3/3/035004.